WORLD RESOURCES INSTITUTE

TECHNICAL NOTE

# AQUEDUCT 3.0: UPDATED DECISION-RELEVANT GLOBAL WATER RISK INDICATORS

RUTGER W. HOFSTE, SAMANTHA KUZMA, SARA WALKER, EDWIN H. SUTANUDJAJA, MARC F.P. BIERKENS, MARIJN J.M. KUIJPER, MARTA FANECA SANCHEZ, RENS VAN BEEK, YOSHIHIDE WADA, SANDRA GALVIS RODRÍGUEZ, AND PAUL REIG

## EXECUTIVE SUMMARY

Water is essential to the progress of human societies. It is required for a healthy environment and a thriving economy. Food production, electricity generation, and manufacturing, among other things, all depend on it.

However, many decision-makers lack the technical expertise to fully understand hydrological information. In response to growing concerns from the private sector and other actors about water availability, water quality, climate change, and increasing demand, WRI applied the composite index approach as a robust communication tool to translate hydrological data into intuitive indicators of water-related risks.

This technical note serves as the main reference for the updated Aqueduct™ water risk framework, in which we combine 13 water risk indicators—including quantity, quality, and reputational risks—into a composite overall water risk score. The main audience for this technical note includes users of the Aqueduct tool, for whom the short descriptions on the tool and in the metadata document are insufficient.

This technical note lays out the design of the Aqueduct water risk framework, explains how various data sources are transformed into water risk indicators, and covers how the indicators are aggregated into composite scores. This document does not explore the differences with the previous version.

## CONTENTS

Executive Summary ..... 1
Introduction ..... 2
1. Water Risk Framework ..... 2
2. Hydrological Model ..... 4
3. Indicators ..... 9
4. Grouped and Overall Water Risk ..... 33
5. Limitations ..... 37
Appendix A: Demand, Withdrawal, and Return Flow ..... 38
Appendix B: Geographic Conversion Table ..... 38
Appendix C: PCR-GLOBWB 2 ..... 39
Appendix D: Delta Sub-basins ..... 47
Endnotes ..... 47
References ..... 48
Acknowledgments ..... 52

*Technical notes document the research or analytical methodology underpinning a publication, interactive application, or tool.*

**Suggested Citation:** Hofste, R., S. Kuzma, S. Walker, E.H. Sutanudjaja, et. al. 2019. "Aqueduct 3.0: Updated Decision-Relevant Global Water Risk Indicators." Technical Note. Washington, DC: World Resources Institute. Available online at: https://www.wri.org/publication/aqueduct-30.

The resulting database and online tools enable comparison of water-related risks across large geographies to identify regions or assets deserving of closer attention. Aqueduct 3.0 introduces an updated water risk framework and new and improved indicators. It also features different hydrological sub-basins. We introduce indicators based on a new hydrological model that now features (1) integrated water supply and demand, (2) surface water and groundwater modeling, (3) higher spatial resolution, and (4) a monthly time series that enables the provision of monthly scores for selected indicators.

Key elements of Aqueduct, such as overall water risk, cannot be directly measured and therefore are not validated. Aqueduct remains primarily a prioritization tool and should be augmented by local and regional deep dives.

# INTRODUCTION

## Background

WRI's Aqueduct™ information platform compiles advances in hydrological modeling, remotely sensed data, and published data sets into a freely accessible online platform.

Since its inception in 2011, the Aqueduct information platform has informed companies, governments, and non-governmental organizations (NGOs) about water-related risks. Since then, the data have been updated regularly, making them comparable on a global scale and accessible to decision-makers worldwide. The Aqueduct information platform contains the following online tools:

- Aqueduct Water Risk Atlas
- Aqueduct Food
- Aqueduct Floods
- Aqueduct Country Rankings

This technical note covers the development of the Aqueduct 3.0 framework and database and serves as the basis of the This technical note covers the development of the Aqueduct 3.0 framework and serves as the basis of the updated Aqueduct Water Risk Atlas online tool.

The updated framework, database, and associated tools improve one of the most widely used and respected water risk frameworks. By leveraging years of experience applying the previous versions and including the latest high-resolution hydrological data sets, we are able to provide a significant update.

## Structure and Scope of This Technical Note

This technical note will first introduce the updated water risk framework (Chapter 1). Many indicators in the framework are based on a new global hydrological model, which is covered in Chapter 2. In Chapter 3, we describe how each of the 13 global water risk indicators is calculated and mapped to a consistent 0–5 scale. Chapter 4 covers how the individual indicators are aggregated into subgroups and an overall water risk score. Chapter 5 lists key limitations.

A comparison to the old framework can be found on WRI's website and is not included in this document.

# 1. WATER RISK FRAMEWORK

## Overview

The water risk framework follows a composite index approach and allows multiple water-related risks to be combined.

There are three hierarchical levels, as can be seen in Figure 1. We start with 13 indicators covering various types of water risk. We then group the indicators and calculate the grouped water risk scores (composite score) using default, industry-defined, or user-defined weighting schemes. Finally, the three groups are combined into a single overall water risk score.

Figure 1 | **Overview of Aqueduct Framework**

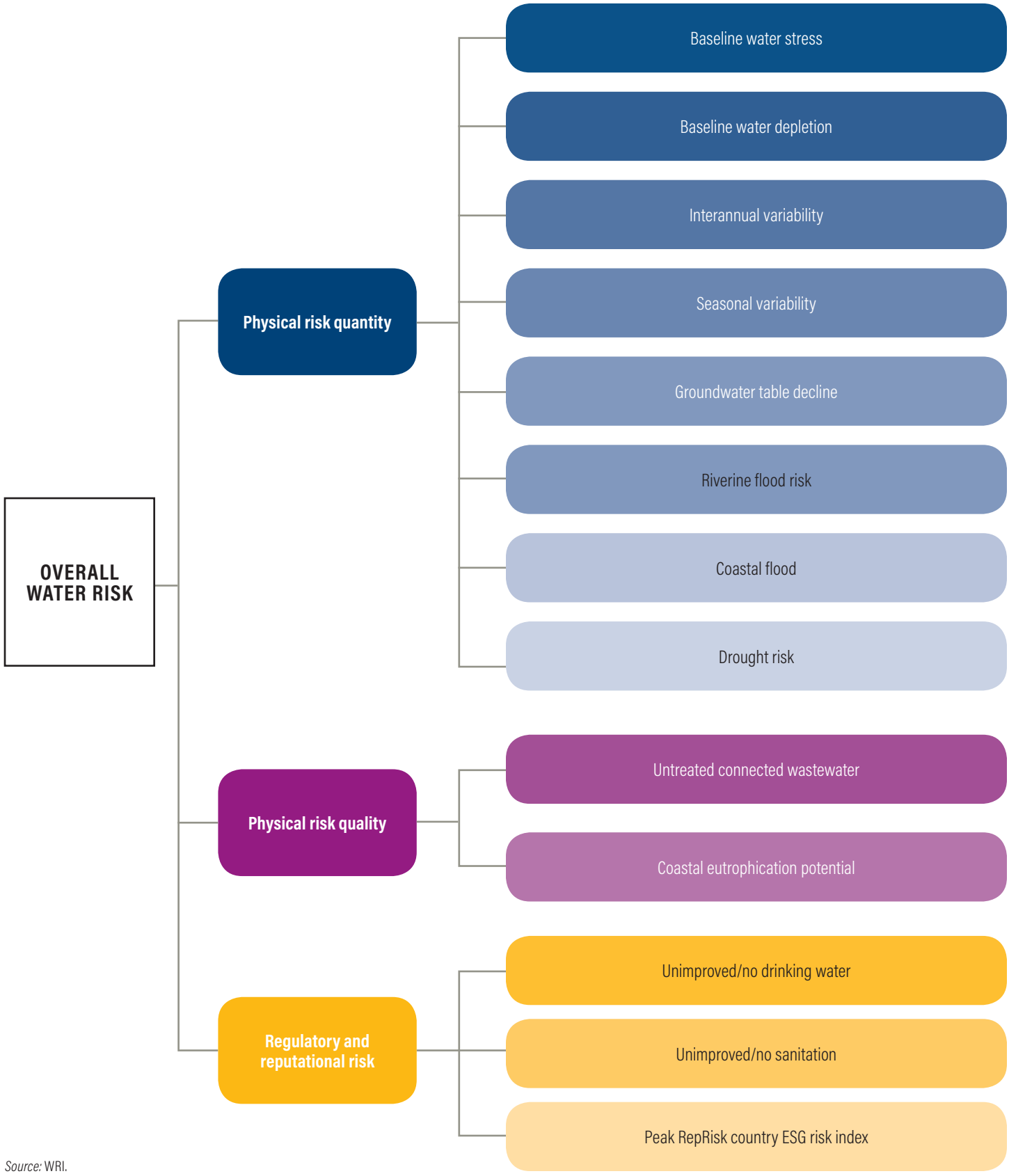


*Source:* WRI.

The rationale for creating a water risk framework is described in WRI's earlier publication: "Aqueduct Water Risk Atlas" (Reig et al. 2013):

> This [water risk] framework organizes indicators into categories of risk that allow the creation of a composite index that brings together multiple dimensions of water-related risk into comprehensive aggregated scores. By providing consistent scores across the globe, the Aqueduct Water Risk Atlas enables rapid comparison across diverse aspects of water risk.
>
> . . .
>
> The Aqueduct Water Risk Framework enables users to study indicators individually or collectively, as well as to quantify and compare a variety of multidimensional water-related measures.

We selected the 13 indicators in Aqueduct 3.0 in three steps:

- We reviewed literature of relevant water issues, existing water indicators, and data sources.
- We evaluated potential data sources through a comparative analysis of their spatial and temporal coverage, granularity, relevance to water users, consistency, and credibility of sources.
- We consulted with industry, public sector, and academic water experts.

We applied the following three principal criteria in selecting indicators:

- They should cover the full breadth of water-related risks, while minimizing overlap and potential confusion resulting from an overabundance of indicators.
- They should be actionable in the context of private and public sector decision-making.
- They should comply with WRI's commitment to open data and transparency—allowing input data, code, and results to be available to anyone who is interested—and be protected under a Creative Commons license 4.0 ("WRI's Open Data Commitment" n.d.).

## 2. HYDROLOGICAL MODEL

Five of the 13 indicators in our framework are based on the outputs of a global hydrological model. Readers interested only in the indicator definitions can proceed directly to Chapter 3. In this chapter, we describe how we have selected the hydrological model and the additional processing steps to make the model output suitable as input for indicator calculation.

From the model's output we use water withdrawal, available water, and groundwater data[1] to calculate baseline water stress, baseline water depletion, seasonal variability, interannual variability, and groundwater table decline (see Table 1).

Table 1 | **Aqueduct Indicators Based on Hydrological Model Output**

| AQUEDUCT INDICATOR | MODEL OUTPUT USED | | |
|---|---|---|---|
| | WATER WITHDRAWAL | AVAILABLE WATER | GROUNDWATER HEADS |
| Baseline water stress | ✓ | ✓ | |
| Baseline water depletion | ✓ | ✓ | |
| Interannual variability | | ✓ | |
| Seasonal variability | | ✓ | |
| Groundwater table decline | | | ✓ |

*Note:* Aqueduct indicators are calculated using the respective outputs of a hydrological model. For example, baseline water depletion is calculated using water withdrawal and available water from the hydrological model.
*Source:* WRI.

## 2.1 Model selection

We considered several global hydrological models and selected the PCRaster Global Water Balance (PCR-GLOBWB 2) model (Wada et al. 2014a; Sutanudjaja et al. 2018) over others, most notably Water Global Assessment and Prognosis (WaterGAP) (Müller Schmied et al. 2014; Eisner 2016) and Global Land Data Assimilation System (GLDAS) Phase 2 (Rodell et al. 2004). At the time the indicators were developed, GLDAS provided information until the year 2012, making it less relevant than PCR-GLOBWB 2 and WaterGAP, both of which could be run for more recent years. There are many similarities between PCR-GLOBWB 2 and WaterGAP. For example, both models run global hydrology and water resources on a global scale at a daily time step; integrate demand, withdrawal, and return flows[2] per time step; include reservoirs; and use kinematic wave routing of river water. Moreover, PCR-GLOBWB 2 can couple to a global two-layer groundwater model (based on MODFLOW) to better represent groundwater flow (de Graaf et al. 2017). The code for PCR-GLOBWB 2 is open source and therefore aligned with WRI's Open Data Commitment ("WRI's Open Data Commitment" n.d.). For these reasons, WRI chose to work with PCR-GLOBWB 2 and use it as the new global hydrological model underpinning Aqueduct.

A description of the model itself and the settings used for Aqueduct 3.0 can be found in Appendix C.

## 2.2 Model output

PCR-GLOBWB 2 is a global, gridded hydrological model. In the case of Aqueduct, each grid cell has a size of 5 × 5 arc minutes. This equates roughly to 10 kilometer (km) × 10 km pixels, with any variation depending on the latitude. We used the following output data from PCR-GLOBWB 2:

#### WITHDRAWAL:

**Gross (consumptive plus nonconsumptive) and net (only consumptive) withdrawal**[3] for four sectors: domestic, industrial, irrigation, and livestock. The (2 x 4=) 8 gridded data sets are available for each month between January 1960 and December 2014.

#### AVAILABLE WATER:

**Accumulated available water**[4] monthly at each grid cell between January 1960 and December 2014.

#### GROUNDWATER HEADS:

Groundwater heads for each month and each grid cell between January 1990 and December 2014.

## 2.3 Processing model output

To make the model output suitable as input for the Aqueduct indicator calculation, we further processed the data by spatial and temporal aggregation.

- Spatial aggregation. Water withdrawal and available water are aggregated to hydrological sub-basins. Groundwater heads are aggregated to aquifers.
- Temporal aggregation. We apply statistical methods to the output time series to get a representative value for the recent situation, while reducing annual anomalies.

### 2.3.1 SPATIAL AGGREGATION

Grid cells are not an appropriate spatial unit to use as input for the Aqueduct indicators. For baseline water stress, baseline water depletion, seasonal variability, and interannual variability, the preferred spatial units are hydrological sub-basins (Gassert et al. 2014). For groundwater table decline, the preferred spatial units are aquifers.

#### HYDROLOGICAL SUB-BASINS

A hydrological basin is an area that drains at a single point to an ocean or inland lake. Each basin can be divided into smaller sub-basins. The assumption is that within each hydrological sub-basin, water resources are pooled. Water withdrawal is satisfied using the water resources available to the sub-basin.

Aqueduct 3.0 uses the HydroBASINS level 6 hydrological sub-basins for three reasons:

- The digital elevation model of HydroBASINS corresponds to PCR-GLOBWB 2.
- HydroBASINS are used in other tools and databases, so comparing and collating data is easier.
- The HydroBASINS sub-basin data set contains 12 levels, ranging from large basins to small sub-basins. In the future, this hierarchical model also will allow flexibility when combining additional data sets (Lehner and Grill 2013).

## AQUIFERS

Groundwater head data are aggregated to groundwater aquifers (BGR and UNESCO 2008). This data set of global aquifers is selected because it has global coverage and is used in the previous version of Aqueduct.

Of the 12 levels, we choose level 6 as the appropriate size of the sub-basins. Water demand is often satisfied with water from a nearby or slightly more distant source. The average distance from source to destination of water supply is the main selection criterion of the appropriate HydroBASINS level. The goal is to select a level large enough to minimize the nonnatural effect of transfers of water ("inter-basin transfer")[5] and small enough to capture meaningful local variations.

Based on limitations, primarily the lack of comprehensive local level inter-basin transfer data in PCR-GLOBWB 2, HydroBASINS level 6 is deemed the most appropriate sub-basin level for Aqueduct 3.0 analysis. For perspective, HydroBASINS level 6 has a median area per sub-basin[6] of 5,318 km² (roughly the size of the U.S. state of Delaware or twice the size of Luxembourg). The distribution of sub-basin areas is depicted in Figure 2.

PCR-GLOBWB 2 and HydroBASINS level 6 both assume a strictly convergent flow. This means that it cannot model bifurcations. This is an issue in delta regions, were rivers tend to split. To address this issue, we have identified delta sub-basins and merged them. The methodology is explained in Appendix D.

### Spatial aggregation of withdrawal data

Sectoral gross and net withdrawal is aggregated to HydroBASINS level 6 by resampling all 5 × 5 arc minute PCR-GLOBWB 2 withdrawal data and the sub-basin delineation to a 30 × 30 arc second grid and calculating the mean flux (i.e., withdrawal in meters per month) per sub-basin.

### Spatial aggregation of available water

PCR-GLOBWB 2 uses a 5 × 5 arc minute spatial resolution, whereas the HydroBASINS sub-basins are derived from a much finer digital elevation model (3 × 3 arc seconds) resampled to 15 × 15 arc second resolution. The result is that the larger 5 × 5 arc minute grid cells might (partially) overlap adjacent sub-basins, thereby erroneously making water available to that sub-basin.

Figure 2 | **Area Distribution of HydroBASIN Level 6**

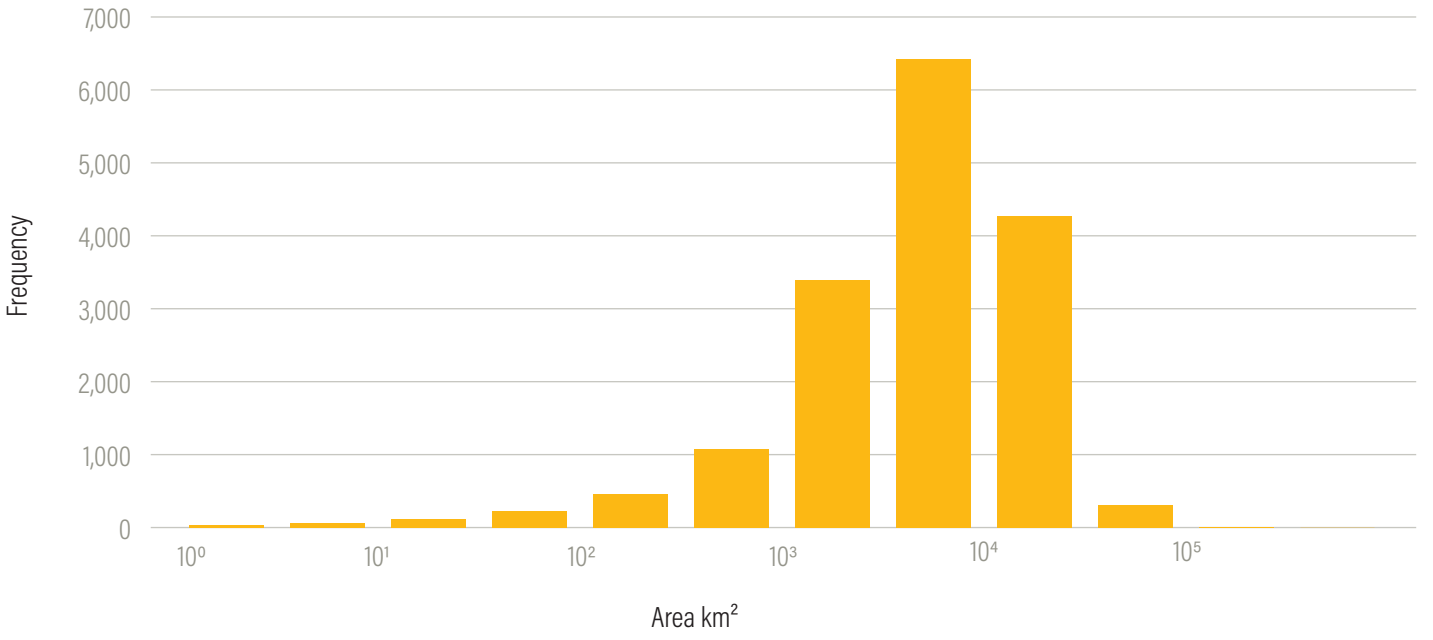

This discrepancy is not an issue when calculating fluxes per sub-basin data, as we did with withdrawal. However, when working with accumulated data, the spatial mismatch can lead to spurious results. We have developed a methodology to address this issue that uses the concept of stream order.

A Strahler stream order (Strahler 1957) is a method of classifying river tributaries based on the nature of confluences. Starting upstream, the smallest stream will be assigned a stream order of 1. When two or more streams with the same stream order converge, the stream order is increased by 1. When multiple streams of different stream orders converge, the stream order of the highest tributary is used (see Figure 3).

Figure 3 | **Strahler Stream Order Schematic**

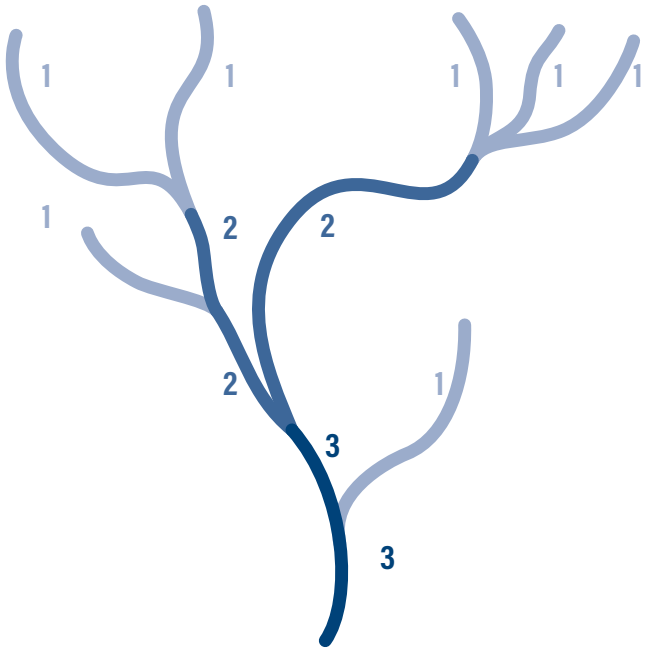


*Source:* WRI, adapted from Strahler 1957

When calculating available water per sub-basin, issues arise when larger 5 × 5 arc minute grid cells intersect adjacent sub-basins, especially near confluences. To address this issue, we apply four steps:

**Step 1: Resample**

The 5 × 5 arc minute PCR-GLOBWB 2 stream order data are resampled to 30 × 30 arc seconds. Each 5 × 5 arc minute cell is now represented by 100 smaller 30 × 30 arc second cells.

**Step 2: Mask**

For each sub-basin, we then create a mask based on two criteria:

- Total number of cells > 1,000
- Number of cells where stream order equals maximum stream order < 150

Only if both criteria are true are the cells with the highest stream order masked.

The second criterion masks cells from an adjacent sub-basin with a higher stream order than the target sub-basin. The threshold is set to 150 to correspond to 1.5 cells at 5 × 5 arc minutes resampled to 30 × 30 arc minutes. In other words, when the sub-basin is sufficiently large and only a small area has the highest stream order, the cells with maximum stream order are masked.

**Step 3: Count maximum available water**

After applying the mask, for each sub-basin, we count the number of cells where available water equals the maximum available water for that sub-basin. If this number is greater than or equal to 100, the value is valid. If not, the second-largest accumulated available water value is used.[7]

**Step 4: Sinks**

Sinks[8] will supersede the masking approach when one or more sinks are present in the sub-basin. This additional requirement is necessary to accurately determine the available water in coastal and inland lake sub-basins.

We apply the approach above to the available water and obtain available water per sub-basin for each month between January 1960 and December 2014.

### 2.3.2 TEMPORAL AGGREGATION

One of the advantages of the Aqueduct framework is its ease of use. Although time series provide detailed insights, for a prioritization method and combined framework, summary indicators are preferred. Aqueduct provides **baseline** water risk information. This is very different from near-real-time water risk information or a historical assessment.[9] Ideally, a baseline is a representation of the current situation without anomalies.

We apply temporal aggregation steps to convert historical time series into useful input for baseline indicator calculations. Groundwater head data are processed separately; see "Groundwater Table Decline" (3.5) for more information.

**Step 1: Total withdrawal**

We calculate the total gross and net withdrawal by summing up the four sectors (domestic, industrial, irrigation, and livestock) for each sub-basin and month (January 1960–December 2014). The results are two time series: Gross total withdrawal and net total withdrawal for January 1960—December 2014 for each sub-basin.

**Step 2: Split months**

We then break up the time series into one series for each month. This yields time series of all months of January between 1960 and 2014, all months of February between 1960 and 2014, and so on to all months of December between 1960 and 2014. We do this for gross total withdrawal, net total withdrawal, and available water.

**Step 3: Regression**

In most sub-basins, the withdrawal data follow a clear increasing trend. This is caused by increases in underlying drivers such as growth in population and gross domestic product (GDP). The data can be erratic, and we try to reduce noise while keeping an accurate representation of the present value.[10] We use ordinary least square (OLS) regression with a trailing moving window size of 10 years.[11] The independent variable is time (year), and the dependent variable is either gross total withdrawal, net total withdrawal, or available water.

Additionally, we restrict the predicted value to the minimum and maximum range of the 10-year moving window values. The predicted value can never exceed the maximum of the 10-year window values or be lower than the minimum of the 10-year window functions.

We opted for a window size of 10 years to capture longer climatic and socioeconomic trends while filtering annual anomalies. The temporal aggregation step 1 through 3 for an example sub-basin is shown in Figure 4.

Figure 4 | **Ordinary Least Square Regression for Total Gross Withdrawal on a 10-Year Moving Window for July in an Example Basin (Ebro Sub-basin (216041)**

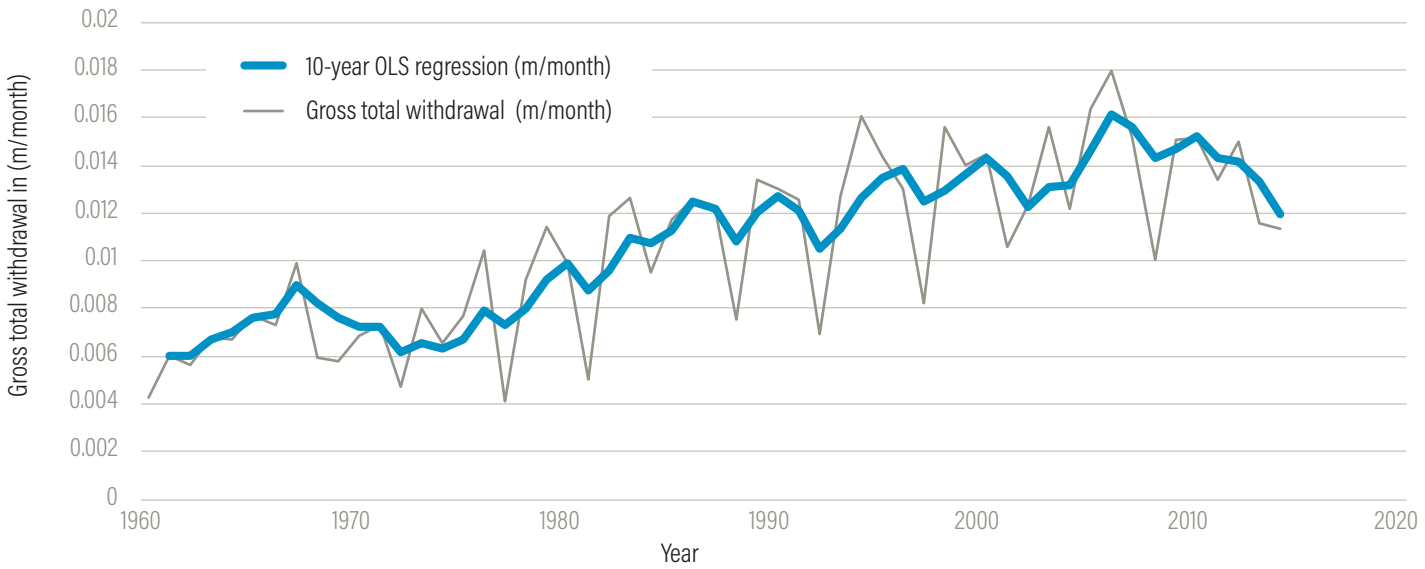


*Source:* WRI.

**Step 4: Mask arid and low water use sub-basins**

**Aqueduct indicators require robust data as inputs.**[12] Sub-basins where data are sparse or very close to zero should therefore be handled separately. We identified those sub-basins using two criteria with thresholds taken from Aqueduct 2.1 (Gassert et al. 2014):

A sub-basin is "arid" if baseline available water < 0.03 meters per year (m/yr)

A sub-basin is "low water use" if baseline gross total withdrawal < 0.012 m/yr

To determine baseline available water and baseline gross total withdrawal, we apply OLS regression to the full time series (1960–2014), instead of 10-year moving windows. This is to prevent different classifications in different years.

#### 2.3.3 PROCESSED WITHDRAWAL AND AVAILABLE WATER

After applying the spatial and temporal aggregation steps, we have gross and net total withdrawal data based on the 10-year OLS regression approach for each sub-basin.

Delta regions and arid and low water use sub-basins will be treated accordingly in the indicator calculation. We use the aggregated time series of gross total withdrawal, net total withdrawal, and available water to calculate baseline water stress, baseline water depletion, seasonal variability, and interannual variability.

## 3. INDICATORS

For each of the 13 indicators in our framework, this chapter offers a description, a calculation of raw values, and a conversion to 0–5 scores. This enables us to aggregate the indicators into groups, as well as to provide an overall water risk score. For each indicator, we also include the key limitations.

Aqueduct 3.0 uses the United Nations Office for Disaster Risk Reduction (UNDRR) risk element terminology of hazard, exposure, and vulnerability. Each indicator is assigned a risk element (see Figure 5):

- **HAZARD:** Threatening event or condition (e.g., flood event, water stress condition).
- **EXPOSURE:** Elements present in the area affected by the hazard (e.g., population, asset, economic value).
- **VULNERABILITY:** The resilience or lack of resilience of the elements exposed to the hazard.

Figure 5 | **Elements of Risk**

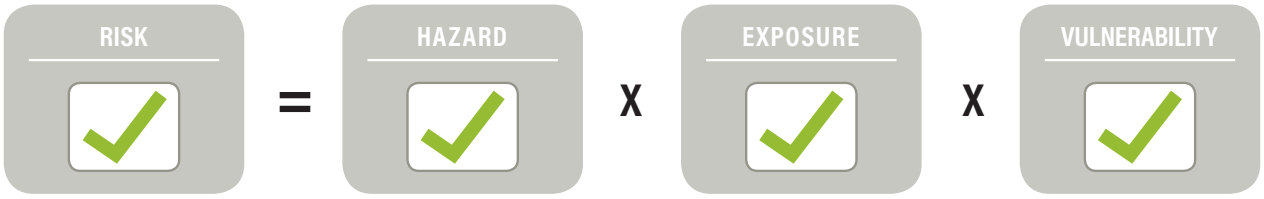


*Source:* Raw data from UNDRR, modified/aggregated by WRI.

## 3.1 Baseline Water Stress

| GENERAL: | |
|---|---|
| **Name** | Baseline Water Stress |
| **Subgroup** | Physical risk quantity |
| **Risk element** | |


| RESULTS: | |
|---|---|
| **Spatial resolution** | Hydrological sub-basin (HydroBASINS 6) |
| **Temporal resolution** | Monthly and annual baseline |

| SOURCE: | |
|---|---|
| **Spatial resolution** | 5 × 5 arc minute grid cells |
| **Temporal resolution** | Monthly |
| **Temporal range** | 1960–2014 |

| EXTRA: | |
|---|---|
| **Partner organization(s)** | Utrecht University |
| **Model** | PCR-GLOBWB 2 |
| **Date of publication** | 2019 |

### 3.1.1 DESCRIPTION

*Baseline water stress* measures the ratio of total water **withdrawals** to available renewable surface and groundwater supplies. Water withdrawals include domestic, industrial, irrigation, and livestock consumptive and nonconsumptive uses. Available renewable water supplies include the impact of upstream consumptive water users and large dams on downstream water availability. **Higher values indicate more competition among users.**

### 3.1.2 CALCULATION

Baseline water stress is calculated using the postprocessed gross and net total withdrawal and available water per sub-basin time series from the default PCR-GLOBWB 2 run (covered in Chapter 2).

**Step 1: Calculate time series of water stress**

$$ws_{m,y,b,ols10} = \frac{ww_{m,y,b,ols10}}{\max(Q_{m,y,b,ols10}) - wn_{m,y,b,ols10}}$$

**IN WHICH,**

$ws_{m,y,b,ols10}$ | Water stress per month, per year, per sub-basin in [-]

$ww_{m,y,b,ols10}$ | Gross (consumptive plus nonconsumptive) total withdrawal per month, per year, per sub-basin in [m/month]

$Q_{m,y,b,ols10}$ | Available water per month, per year, per sub-basin in [m/month]

$wn_{m,y,b,ols10}$ | Net (consumptive) total withdrawal per month, per year, per sub-basin in [m/month]

This results in 12 time series of water stress (one for each month) per sub-basin. Note that water resources in delta sub-basins are pooled.

**Step 2: Determine baseline water stress**

Another OLS regression is fitted through the water stress time series. The regression value for the year 2014 is used as a baseline. Note that, although we use the "2014" value of the regression, this is not an estimate of the water stress in 2014. Instead, the result of this approach is a baseline.

$$bws_{m,s} = OLS(ws_{m,y,b,ols10})_{2014}$$

**IN WHICH,**

$bws_{m,s}$ | Raw value of baseline water stress per month per sub-basin in [-]

$ws_{m,y,b,ols10}$ | Water stress per month, per year, per sub in [-]

The result is 12 water stress values, one for each month. Additionally, we limit the raw values to a maximum of 1 and a minimum of 0. We calculate the annual water stress by averaging the monthly values.

Sub-basins classified as "arid and low water use" are handled separately.

### 3.1.3 CONVERSION TO RISK CATEGORIES

The risk thresholds are based on Aqueduct 2.1 (Gassert et al. 2014).

| RAW VALUE | RISK CATEGORY | SCORE |
|---|---|---|
| <10% | Low | 0–1 |
| 10–20% | Low–medium | 1–2 |
| 20–40% | Medium–high | 2–3 |
| 40–80% | High | 3–4 |
| >80% | Extremely high | 4–5 |
| | Arid and low water use | 5 |

The raw values are remapped to a 0–5 scale using the following equation:

$$score = \max\left(0, min\left(5, \frac{ln(r) - ln(0.1)}{ln(2)} + 1\right)\right)$$

Where *r* is the raw indicator value and *score* is the indicator score [0–5].

### 3.1.4 LIMITATIONS

All limitations of the underlying data, including those produced by the PCR-GLOBWB 2 global hydrological model and HydroBASINS 6 hydrological sub-basin delineation, apply to this indicator. Please see the original publications of these data sets for a full list of limitations.

One of the biggest assumptions is that water resources are pooled within each sub-basin. However, in HydroBASINS 6, coastal and island sub-basins are often grouped to make the area of the sub-basins more homogeneous. The assumption of shared water resources might not hold in aggregated coastal sub-basins.

Water resources in PCR-GLOBWB 2 are pooled in abstraction zones. This assumption differs from the sub-basin approach in Aqueduct. This is one of the prime reasons for further processing of the PCR-GLOBWB 2 data.

Although the underlying models have been validated, the results are not. Water stress remains subjective and cannot be measured directly. The lack of direct validation makes it impossible to assess some of the parameters in our calculation, such as the length of the input time series, regression method, and optimal moving window size.

The water stress indicator presented here does not explicitly take into account environmental flow requirements,[13] water quality, or access to water. Views differ regarding what to include in a water stress indicator (Vanham et al. 2018).

Finally, we should stress that Aqueduct is tailored to large-scale comparison of water-related risks. The indicators have limited added value on a local scale.

## 3.2 Baseline Water Depletion

| GENERAL: | |
|---|---|
| **Name** | Baseline Water Depletion |
| **Subgroup** | Physical risk quantity |
| **Risk element** | |


| RESULTS: | |
|---|---|
| **Spatial resolution** | Hydrological sub-basin (HydroBASINS 6) |
| **Temporal resolution** | Monthly and annual baseline |

| SOURCE: | |
|---|---|
| **Spatial resolution** | 5 × 5 arc minute grid cells |
| **Temporal resolution** | Monthly |
| **Temporal range** | 1960–2014 |

| EXTRA: | |
|---|---|
| **Partner organization(s)** | Utrecht University |
| **Model** | PCR-GLOBWB 2 |
| **Date of publication** | 2019 |

### 3.2.1 DESCRIPTION

*Baseline water depletion* measures the ratio of total water **consumption** to available renewable water supplies. Total water consumption includes domestic, industrial, irrigation, and livestock consumptive uses. Available renewable water supplies include the impact of upstream consumptive water users and large dams on downstream water availability. **Higher values indicate larger impact on the local water supply and decreased water availability for downstream users.**

Baseline water depletion is similar to baseline water stress; however, instead of looking at total water withdrawal (consumptive plus nonconsumptive), baseline water depletion is calculated using consumptive withdrawal only.

### 3.2.2 CALCULATION

Baseline water depletion is calculated using the processed net total withdrawal and available water per sub-basin time series from the default PCR-GLOBWB 2 run (covered in Chapter 2).

**Step 1: Calculate time series of water depletion**

$$wd_{m,y,b,ols10} = \frac{wn_{m,y,b,ols10}}{\max(Q_{m,y,b,ols10}) - wn_{m,y,b,ols10}}$$

**IN WHICH,**

$wd_{m,y,b,ols10}$ | Water depletion per month, per year, per sub-basin in [-]

$wn_{m,y,b,ols10}$ | Net (consumptive) total withdrawal per month, per year, per sub-basin in [m/month]

$Q_{m,y,b,ols10}$ | Available water per month, per year, per sub-basin in [m/month]

This results in 12 time series of water depletion (one for each month) per sub-basin. Note that water resources in delta sub-basins are pooled (shared).

**Step 2: Determine baseline water depletion**

Another OLS regression is fitted through the water depletion time series. The regression value for the year 2014 is used as a baseline. Note that, although we use the "2014" value of the regression, this is not an estimate of the water depletion in 2014. Instead, the result of this approach is a baseline.

$$bwd_{m,s} = OLS(wd_{m,y,b,ols10})_{2014}$$

**IN WHICH,**

$bwd_{m,s}$ | Raw value of baseline water depletion per month per sub-basin in [-]

$wd_{m,y,b,ols10}$ | Water depletion per month, per year, per sub in [-]

This results in 12 water depletion values, one for each month. Additionally, we limit the raw values to a maximum of 1 and a minimum of 0. We calculate the annual water depletion by averaging the monthly values.

Sub-basins classified as "arid and low water use" are handled separately.

### 3.2.3 CONVERSION TO RISK CATEGORIES

The thresholds are based on Brauman et al. (2016).

| RAW VALUE | RISK CATEGORY | SCORE |
|---|---|---|
| <5% | Low | 0–1 |
| 5–25% | Low–medium | 1–2 |
| 25–50% | Medium–high | 2–3 |
| 50–75% | High | 3–4 |
| >75% | Extremely high | 4–5 |
| | Arid and low water use | 5 |

We use linear interpolation within each category to remap the raw values to a 0–5 scale using the following equation:

$$score = \begin{cases} \max(20r, 0), & r < 0.05 \\ 5r + \frac{3}{4}, & 0.05 \leq r < 0.25 \\ min(5, r4 + 1), & r \geq 0.25 \end{cases}$$

Where *r* is the raw indicator value and *score* is the indicator score [0–5].

### 3.2.4 LIMITATIONS

See Baseline Water Stress, Limitations (3.1.4).

In addition, we had to omit the categories "dry year" and "seasonal" from Brauman et al. (2016) to make the indicator suitable for the Aqueduct framework.

## 3.3 Interannual Variability

| GENERAL: | |
|---|---|
| **Name** | Interannual Variability |
| **Subgroup** | Physical risk quantity |
| **Risk element** | |


| RESULTS: | |
|---|---|
| **Spatial resolution** | Hydrological sub-basin (HydroBASINS 6) |
| **Temporal resolution** | Monthly and annual baseline |

| SOURCE: | |
|---|---|
| **Spatial resolution** | 5 × 5 arc minute grid cells |
| **Temporal resolution** | Monthly |
| **Temporal range** | 1960–2014 |

| EXTRA: | |
|---|---|
| **Partner organization(s)** | Utrecht University |
| **Model** | PCR-GLOBWB 2 |
| **Date of publication** | 2019 |

### 3.3.1 DESCRIPTION

*Interannual variability* measures the average between-year variability of available water supply, including both renewable surface and groundwater supplies. **Higher values indicate wider variations in available supply from year to year.**

### 3.3.2 CALCULATION

Interannual variability is calculated using the available water time series from the default PCR-GLOBWB 2 aggregated in space but not in time. See Chapter 2.

Interannual, or between year, variability is defined as the coefficient of variation (CV) of available water for each sub-basin. The CV is the standard deviation (SD) of the available water, divided by the mean. The CV per sub-basin is determined for each individual month, as well as annually.

$$iav_{m,b} = cv_{m,b} = \frac{SD_{1960-2014}(Q_{m,b})}{mean_{1960-2014}(Q_{m,b})}$$

**IN WHICH,**

$cv_{m,b}$ | Coefficient of variation per month, per sub-basin [-]

$Q_{m,b}$ | Available water per month, per sub-basin in meters per year

$iav_{m,b}$ | Interannual variability per month, per sub-basin in [-]

### 3.3.3 CONVERSION TO RISK CATEGORIES

The risk thresholds are based on Aqueduct 2.1 (Gassert et al. 2014).

| RAW VALUE | RISK CATEGORY | SCORE |
|---|---|---|
| <0.25 | Low | 0–1 |
| 0.25–0.50 | Low–medium | 1–2 |
| 0.50–0.75 | Medium–high | 2–3 |
| 0.75–1.00 | High | 3–4 |
| >1.00 | Extremely high | 4–5 |

The raw values are remapped to a 0–5 scale using the following equation:

$$score = max(0, min(5, 4r))$$

Where $r$ is the raw indicator value and *score* is the indicator score [0–5].

### 3.3.4 LIMITATIONS

See Baseline Water Stress, Limitations (3.1.4).

In addition, we have analyzed the full time series of PCR-GLOBWB 2; that is, 1960 to 2014. We have not analyzed the effect of using a different range.

## 3.4 Seasonal Variability

| GENERAL: | |
|---|---|
| **Name** | Seasonal Variability |
| **Subgroup** | Physical risk quantity |
| **Risk element** | |


| RESULTS: | |
|---|---|
| **Spatial resolution** | Hydrological sub-basin (HydroBASINS 6) |
| **Temporal resolution** | Annual baseline |

| SOURCE: | |
|---|---|
| **Spatial resolution** | 5 × 5 arc minute grid cells |
| **Temporal resolution** | Monthly |
| **Temporal range** | 1960–2014 |

| EXTRA: | |
|---|---|
| **Partner organization(s)** | Utrecht University |
| **Model** | PCR-GLOBWB 2 |
| **Date of publication** | 2019 |

### 3.4.1 DESCRIPTION

*Seasonal variability* measures the average within-year variability of available water supply, including both renewable surface and groundwater supplies. **Higher values indicate wider variations of available supply within a year.**

### 3.4.2 CALCULATION

Seasonal variability is calculated using the available water time series from the default PCR-GLOBWB aggregated in space but not in time. See Chapter 2.

First, the available water per month, per sub basin, is calculated over the entire time series 1960–2014 (55 years).

$$\bar{Q}_{m,b} = \frac{1}{55}\sum_{y=1960}^{2014} Q_{y,m,b}, m \in \{jan \dots dec\}$$

**IN WHICH,**

$Q_{m,b}$ | Average available water per month per sub-basin in [m/month]

$Q_{y,m,b}$ | Available water per year per month per sub-basin in [m/month]

The coefficient of variation is calculated using these 12 averages.

$$sev_b = \frac{SD_{[Jan\dots Dec]}(\bar{Q}_{m,b})}{mean_{[Jan\dots Dec]}(\bar{Q}_{m,b})}$$

**IN WHICH,**

$sev_b$ | Seasonal variability per sub-basin in [-]

$Q_{m,b}$ | Average available water per month per sub-basin in [m/month]

### 3.4.3 CONVERSION TO RISK CATEGORIES

The risk thresholds are based on Aqueduct 2.1 (Gassert et al. 2014).

| RAW VALUE | RISK CATEGORY | SCORE |
|---|---|---|
| <0.33 | Low | 0–1 |
| 0.33–0.66 | Low–medium | 1–2 |
| 0.66–1.00 | Medium–high | 2–3 |
| 1.00–1.33 | High | 3–4 |
| >1.33 | Extremely high | 4–5 |

The raw values are remapped to a 0–5 scale using the following equation:

$$score = max\big(0, min(5{,}3r)\big)$$

Where *r* is the raw indicator value and *score* is the indicator score [0–5].

### 3.4.4 LIMITATIONS

See Baseline Water Stress, Limitations (3.1.4).

Additionally, the effect of using different lengths of the input time series is not examined. The human and climatic influence on available water is likely to be more profound in recent years.

## 3.5 Groundwater Table Decline

| GENERAL: | |
|---|---|
| **Name** | Groundwater Table Decline |
| **Subgroup** | Physical risk quantity |
| **Risk element** | |


| RESULTS: | |
|---|---|
| **Spatial resolution** | Groundwater aquifer (WHYMAP) |
| **Temporal resolution** | Annual baseline |

| SOURCE: | |
|---|---|
| **Spatial resolution** | 5 × 5 arc minute grid cells |
| **Temporal resolution** | Monthly |
| **Temporal range** | 1960–2014 |

| EXTRA: | |
|---|---|
| **Partner organization(s)** | Deltares, Utrecht University |
| **Model** | PCR-GLOBWB 2 + MODLFOW |
| **Date of publication** | 2019 |

### 3.5.1 DESCRIPTION

*Groundwater table decline* measures the average decline of the groundwater table as the average change for the period of study (1990–2014). The result is expressed in centimeters per year (cm/yr). **Higher values indicate higher levels of unsustainable groundwater withdrawals.**

### 3.5.2 CALCULATION

Groundwater table decline is calculated using the groundwater heads time series from the PCR-GLOBWB 2 run coupled with MODFLOW to account for lateral groundwater flow processes. This indicator is based on the gridded[14] monthly groundwater heads between January 1990 and December 2014.[15]

The groundwater aquifers contain several geomorphological features, which for practical reasons can be divided into sedimentary basins and mountain ranges. In mountainous areas, most materials are hard rock and eventually weathered. In the PCR-GLOBWB 2 model coupled with MODFLOW, very deep groundwater influences the averages in mountainous cells and is not representative. These cells are therefore discarded from the calculations following the method in de Graaf et al. (2015).

Mountainous areas are determined by comparing the height of the floodplain within a cell with the average elevation of that same cell. The elevation of the floodplain is derived from the 30 × 30 arc second digital elevation data from HydroSheds (Lehner et al. 2008). The flood plain elevation is simply the minimum of the input.

$$h_{floodplain,5'} = \min(h_{DEM\ 30''})$$

**IN WHICH,**

$h_{floodplain,5'}$ | Elevation of floodplain in meters for each 5 × 5 arc minute cell

$h_{DEM\ 30''}$ | Elevation derived from 30 × 30 arc second digital elevation model (DEM) in meters

The average elevation for each 5-arc minute cell is taken directly from the HydroSheds data. If the difference between the floodplain elevation and the average elevation is greater than 50 m, the cell is classified as mountainous.

$$\text{mountainous} = \begin{cases} True, \ if \ (h_{DEM,5'} - h_{floodplain,5'}) > 50m \\ False, \ otherwise \end{cases}$$

**IN WHICH,**

$h_{floodplain,5'}$ | Elevation of floodplain in meters

$h_{DEM\ 5'}$ | Elevation derived from 5 arc minute (approximately 11 km at equator) DEM in meters

The threshold of 50 m was chosen as it proved to include 70 percent of the unconsolidated sediments mapped in the Global Lithological Map (Hartmann and Moosdorf 2012).

After masking the mountainous areas, results are aggregated to groundwater aquifers derived from the Worldwide Hydrogeological Mapping and Assessment Programme (WHYMAP) data set (BGR and UNESCO 2018).

The monthly results at the aquifer scale are fitted with a first-order regression. The slope of this regression line (cm/yr) indicates the existence of a downward (or upward) trend. The following estimators are used to further assess the trend: (1) coefficient of determination and (2) the *p value*.

The coefficient of determination is used to determine whether the trend is linear or erratic. A minimum threshold of 0.9 is applied to mask out erratic and error-prone trends.

For the *p value, a maximum threshold of 0.05 is used.*

$$valid = \begin{cases} True, \ if \ R^2 \geq 0.9 \ and \ p \leq 0.05 \\ False, \ otherwise \end{cases}$$

### 3.5.3 CONVERSION TO RISK CATEGORIES

The risk category thresholds are based on a combination of expert judgment and a literature review (Galvis Rodríguez et al. 2017).

| RAW VALUE | RISK CATEGORY | SCORE |
|---|---|---|
| <0 cm/y | Low | 0–1 |
| 0–2 cm/y | Low–medium | 1–2 |
| 2–4 cm/y | Medium–high | 2–3 |
| 4–8 cm/y | High | 3–4 |
| >8 cm/y | Extremely high | 4–5 |

Within each category, we use linear interpolation to convert the raw values to a 0–5 scale using the following equation:

$$score = \begin{cases} max(r+1,0), & r < 0 \\ r+1, & 0 \leq r < 2 \\ \frac{1}{2}r+1, & 2 \leq r < 8 \\ \min\left(5, \frac{1}{2}r+1\right), & r \geq 8 \end{cases}$$

Where *r* is the raw indicator value and *score* is the indicator score [0–5].

### 3.5.4 LIMITATIONS

The limitations of PCR-GLOBWB 2, MODFLOW, WHYMAP, climate forcing, and other input data sets are propagated to these results. The results are only validated using a literature review of selected aquifers and by comparing the results to coarse remote-sensing data.

The threshold for masking out mountainous areas was set once without a sensitivity analysis. The temporal range [1990–2014] was selected on the basis of expert judgment and differs from some of the other water quantity indicators that use [1960–2014] as the input time series.

See Galvis Rodríguez et al. (2017) for additional limitations.

## 3.6 Riverine Flood Risk

| GENERAL: | |
|---|---|
| **Name** | Riverine Flood Risk |
| **Subgroup** | Physical risk quantity |
| **Risk element** | |


| RESULTS: | |
|---|---|
| **Spatial resolution** | Hydrological sub-basin (HydroBASINS 6) |
| **Temporal resolution** | Annual baseline |

| SOURCE: | |
|---|---|
| **Spatial resolution** | 30 × 30 arc minute grid cells |
| **Temporal resolution** | Annual |
| **Temporal range** | 2010 |

| EXTRA: | |
|---|---|
| **Partner organization(s)** | Deltares, IVM, PBL, Utrecht University |
| **Model** | GLOFRIS (Ward et al. forthcoming) |
| **Date of publication** | 2019 |

| ADDITIONAL DATA SOURCE | INPUT SPATIAL RESOLUTION | INPUT TEMPORAL RESOLUTION | INPUT TEMPORAL RANGE | SOURCE |
|---|---|---|---|---|
| Existing Flood Protection Levels | State | Annual | 2016 | FLOPROS (Scussolini et al. 2016) |

### 3.6.1 DESCRIPTION

*Riverine flood risk* measures the percentage of population expected to be affected by riverine flooding in an average year, accounting for existing flood-protection standards. Flood risk is assessed using hazard (inundation caused by river overflow), exposure (population in flood zone), and vulnerability.[16] The existing level of flood protection is also incorporated into the risk calculation. It is important to note that this indicator represents flood risk not in terms of maximum possible impact but rather as average annual impact. The impacts from infrequent, extreme flood years are averaged with more common, less newsworthy flood years to produce the "expected annual affected population." **Higher values indicate that a greater proportion of the population is expected to be impacted by riverine floods on average.**

### 3.6.2 CALCULATION

Data on the population impacted by riverine floods are provided by Aqueduct Floods at the state/HydroBASIN 6 intersect scale (Ward et al. forthcoming). The data set estimates the average number of people to be impacted annually for several flood event magnitudes (2, 5, 10, 25, 50, 100, 250, 500, and 1,000 in return periods).

The *expected annual affected population* is calculated using a risk curve (Meyer et al. 2009). To create the curve, the return periods are first converted into probabilities (i.e., 1/return period) and then plotted on the *x* axis against the impacted population (Figure 6). Next, flood protection is added to the graph. The current level of flood protection, given in return years, comes from the Flood Protection Standards (FLOPROS) model (Scussolini et al. 2016). All impacts that fall to the right of the flood protection line (i.e., impacted by smaller floods) are assumed to be protected against floods and are removed from the calculation. The *expected annual affected population* is calculated by integrating the area under the curve *to the left* of the flood protection line.

The *expected annual affected population* is calculated for each state/HydroBASIN 6 intersect, then aggregated up to the HydroBASIN 6 scale. The *total population* in each state/HydroBASIN 6 intersect is also summed to the HydroBASIN 6 scale (Ward et al. forthcoming). Finally, the raw riverine flood risk score—the *percentage of popu-*

Figure 6 | **Risk Curve Used to Calculate Expected Annual Affected Population from Floods**

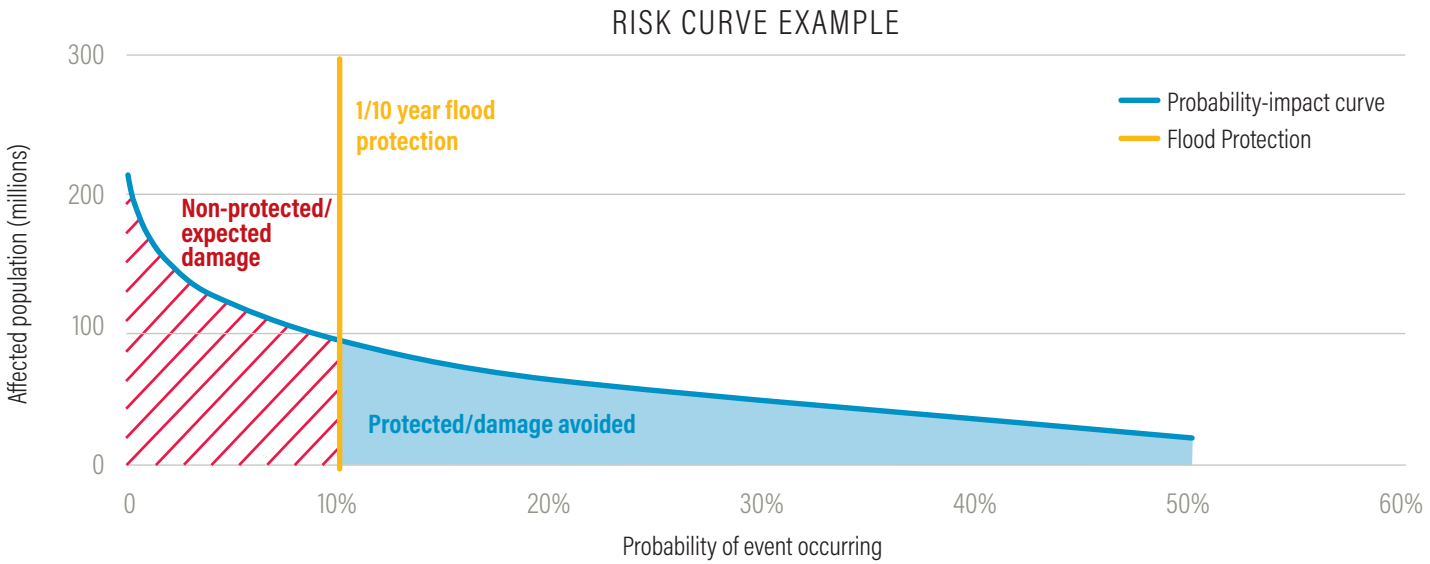


*Source:* WRI.

*lation expected to be affected annually by riverine floods* per HydroBASIN 6—is calculated:

$$rfr = \frac{pop_{exp,r,y}}{pop_{tot}}$$

**IN WHICH,**

*rfr* | Riverine flood risk raw value in [-]

$pop_{exp,r,y}$ | Expected annual affected population by riverine flooding in [number of people]

### 3.6.3 CONVERSION TO RISK CATEGORIES

The thresholds are based on quantiles, with the exception of the basins with no riverine hazard. Basins without a flood hazard are given the lowest risk score, 0, and are removed from the rest of the data set before the quantiles are calculated.

| RAW VALUE | RISK CATEGORY | SCORE |
|---|---|---|
| 0 to 1 in 1,000 | Low | 0–1 |
| 1 in 1,000 to 2 in 1,000 | Low–medium | 1–2 |
| 2 in 1,000 to 6 in 1,000 | Medium–high | 2–3 |
| 6 in 1,000 to 1 in 100 | High | 3–4 |
| More than 1 in 100 | Extremely high | 4–5 |

The raw values are remapped to a 0–5 scale using the following equation:

$$score = \begin{cases} \frac{r-0}{0.12\%-0}, & r < 0.12\% \\ \frac{r-0.12\%}{0.30\%-0.12\%} + 1, & 0.12\% \le r < 0.30\% \\ \frac{r-0.30\%}{0.62\%-0.30\%} + 2, & 0.30\% \le r < 0.62\% \\ \frac{r-0.62\%}{1.3\%-0.62\%} + 3, & 0.62\% \le r < 1.3\% \\ \frac{r-1.3\%}{\max(r_{all})-1.3\%} + 4, & r \ge 1.3\% \end{cases}$$

Where *r* is the raw indicator value and *score* is the indicator score [0–5].

### 3.6.4 LIMITATIONS

Riverine and coastal flood risks must be evaluated and used separately, as the compound risks between river and storm surges are not modeled. The data also assume that flood events are entirely independent of each other, so the impact from overlapping flood events is not considered. Finally, the data do not include any indirect impacts from flooding (e.g., disrupted transportation, loss of work, etc.).

## 3.7 Coastal Flood Risk

| GENERAL: | |
|---|---|
| **Name** | Coastal Flood Risk |
| **Subgroup** | Physical risk quantity |
| **Risk element** | |


| RESULTS: | |
|---|---|
| **Spatial resolution** | Hydrological sub-basin (HydroBASINS 6) |
| **Temporal resolution** | Annual baseline |

| SOURCE: | |
|---|---|
| **Spatial resolution** | 30 × 30 arc minute grid cells |
| **Temporal resolution** | Annual |
| **Temporal range** | 2010 |

| EXTRA: | |
|---|---|
| **Partner organization(s)** | Deltares, IVM, PBL, Utrecht University |
| **Model** | GLOFRIS (Ward et al. forthcoming) |
| **Date of publication** | 2019 |

| ADDITIONAL DATA SOURCE | INPUT SPATIAL RESOLUTION | INPUT TEMPORAL RESOLUTION | INPUT TEMPORAL RANGE | SOURCE |
|---|---|---|---|---|
| Existing Flood Protection Levels | State | Annual | 2016 | FLOPROS (Scussolini et al. 2016) |

### 3.7.1 DESCRIPTION

*Coastal flood risk* measures the percentage of the population expected to be affected by coastal flooding in an average year, accounting for existing flood protection standards. Flood risk is assessed using hazard (inundation caused by storm surge), exposure (population in flood zone), and vulnerability.[17] The existing level of flood protection is also incorporated into the risk calculation. It is important to note that this indicator represents flood risk not in terms of maximum possible impact but rather as average annual impact. The impacts from infrequent, extreme flood years are averaged with more common, less newsworthy flood years to produce the "expected annual affected population." **Higher values indicate that a greater proportion of the population is expected to be impacted by coastal floods on average.**

### 3.7.2 CALCULATION

Data on the population impacted by coastal floods are provided by Aqueduct Floods at the state/HydroBASIN 6 intersect scale (Ward et al. forthcoming). The data set estimates the average number of people to be impacted annually for several flood event magnitudes (2, 5, 10, 25, 50, 100, 250, 500, and 1,000 in return periods).

The *expected annual affected population* is calculated using a risk curve (Meyer et al. 2009). To create the curve, the return periods are first converted into probabilities (i.e., 1/return period) and then plotted on the *x* axis against the impacted population (Figure 6). Next, vulnerability—or flood protection—is added to the graph as a vertical line. The current level of flood protection, given in return years, comes from the FLOPROS model (Scussolini et al. 2016). All impacts that fall to the right of the flood protection line (i.e., impacted by smaller floods) are assumed to be protected against floods and are removed from the calculation. The *expected annual affected population* is calculated by integrating the area under the curve *to the left* of the flood protection line.

The *expected annual affected population* is calculated for each state/HydroBASIN 6 intersect and then aggregated up to the HydroBASIN 6 scale. The *total population* in each state/HydroBASIN 6 intersect is also summed to the HydroBASIN 6 scale (Ward et al. forthcoming). Finally, the raw coastal flood risk score—the *percentage of population expected to be affected annually by coastal floods* per HydroBASIN 6—is calculated:

$$cfr = \frac{pop_{exp,c,y}}{pop_{tot}}$$

**IN WHICH,**

*cfr* | Coastal flood risk raw value in [-]

$pop_{exp,c,y}$ | Expected annual affected population by coastal flooding in [number of people]

### 3.7.3 CONVERSION TO RISK CATEGORIES

The thresholds are based on quantiles, with the exception of the basins with no coastal hazard. Basins without a flood hazard are given the lowest risk score, 0, and removed from the rest of the data set before the quantiles are calculated.

| RAW VALUE | RISK CATEGORY | SCORE |
|---|---|---|
| 0 to 9 in 1,000,000 | Low | 0–1 |
| 9 in 1,000,000 to 7 in 100,000 | Low–medium | 1–2 |
| 7 in 100,000 to 3 in 10,000 | Medium–high | 2–3 |
| 3 in 10,000 to 2 in 1,000 | High | 3–4 |
| More than 2 in 1,000 | Extremely high | 4–5 |

The raw values are remapped to a 0–5 scale using the following equation:

$$score = \begin{cases} \frac{r-0}{0.001\%-0}, & r < 0.001\% \\ \frac{r-0.001\%}{0.007\%-0.001\%} + 1, & 0.001\% \leq r < 0.007\% \\ \frac{r-0.007\%}{0.0.04\%-0.007\%} + 2, & 0.007\% \leq r < 0.04\% \\ \frac{r-0.04\%}{0.22\%-0.04\%} + 3, & 0.04\% \leq r < 0.22\% \\ \frac{r-0.22\%}{\max(r_{all})-0.22\%} + 4, & r \geq 0.22\% \end{cases}$$

Where *r* is the raw indicator value and *score* is the indicator score [0–5].

### 3.7.4 LIMITATIONS

Riverine and coastal flood risks must be evaluated and used separately, as the compound risks between river and storm surges are not modeled. The data also assume that flood events are entirely independent of each other, so the impact from overlapping flood events is not considered. Finally, the data do not include any indirect impacts from flooding (e.g., disrupted transportation, loss of work, etc.).

## 3.8 Drought Risk

| GENERAL: | |
|---|---|
| **Name** | Drought Risk |
| **Subgroup** | Physical risk quantity |
| **Risk element** | |


| RESULTS: | |
|---|---|
| **Spatial resolution** | Hydrological sub-basin (HydroBASINS 6) |
| **Temporal resolution** | Annual baseline |

| SOURCE: | |
|---|---|
| **Spatial resolution** | 5 × 5 arc minute grid cells |
| **Temporal resolution** | Annual |
| **Temporal range** | 2000–2014 |

| EXTRA: | |
|---|---|
| **Partner organization(s)** | JRC |
| **Model** | Various |
| **Date of publication** | 2016 |

### 3.8.1 DESCRIPTION

*Drought risk measures* where droughts are likely to occur, the population and assets exposed, and the vulnerability of the population and assets to adverse effects. **Higher values indicate higher risk of drought.**

### 3.8.2 CALCULATION

The drought risk indicator is based on Carrão et al. (2016) and is used with minimal alterations. Drought risk is assessed for the period 2000–2014 and is a combination of drought hazard, drought exposure, and drought vulnerability.

Risk = hazard × exposure × vulnerability

The methodology is explained in Carrão et al. (2016):

> Drought hazard is derived from a non-parametric analysis of historical precipitation deficits at the 0.5 [degree resolution]; drought exposure is based on a non-parametric aggregation of gridded indicators of population and livestock densities, crop cover and water stress; and drought vulnerability is computed as the arithmetic composite of high level factors of social, economic and infrastructural indicators, collected at both the national and sub-national levels.

The hazard, exposure, vulnerability, risk, and no-data mask data available at 5 × 5 arc minute resolution are averaged for each hydrological sub-basin.

$$dr_{subbasin} = \frac{1}{n_{pix}} \sum_{i=1}^{n_{pix}} dr_{pix}$$

**IN WHICH,**

$dr_{sub\text{-}basin}$ | Drought risk per sub-basin

$n_{pix}$ | Number of pixels per sub-basin

$dr_{pix}$ | Drought risk per pixel

### 3.8.3 CONVERSION TO RISK CATEGORIES

The risk categories are derived from Carrão et al. (2016):

| RAW VALUE | RISK CATEGORY | SCORE |
|---|---|---|
| 0.0–0.2 | Low | 0–1 |
| 0.2–0.4 | Low–medium | 1–2 |
| 0.4–0.6 | Medium | 2–3 |
| 0.6–0.8 | Medium–high | 3–4 |
| 0.8–1.0 | High | 4–5 |

The raw values are remapped to a 0–5 scale using the following equation:

$$score = 5r$$

Where $r$ is the raw indicator value and *score* is the indicator score [0–5].

### 3.8.4 LIMITATIONS

Many of the indicators in the Aqueduct water risk framework represent a hazard. Some indicators, including drought risk, add exposure and vulnerability. Aqueduct combines these risk elements into a single framework.

The drought risk indicator does not consider hydrological drought and excludes associated risks such as unnavigable rivers.

Other Aqueduct risk categories are typically skewed toward the higher side, with the category "extremely high" as the top category. The drought risk indicator has not been interpreted yet and is therefore presented at a low–high scale instead of low–extremely high.

See Carrão et al. (2016) for limitations of the different risk elements (hazard, exposure, vulnerability) and the input data sets.

## 3.9 Untreated Connected Wastewater

| GENERAL: | |
|---|---|
| **Name** | Untreated Connected Wastewater |
| **Subgroup** | Physical risk quality |
| **Risk element** | |


| RESULTS: | |
|---|---|
| **Spatial resolution** | Country |
| **Temporal resolution** | Annual baseline |

| SOURCE: | |
|---|---|
| **Spatial resolution** | Country |
| **Temporal resolution** | Annual |
| **Temporal range** | 2000–2010 |

| EXTRA: | |
|---|---|
| **Partner organization(s)** | IFPRI, Veolia |
| **Model** | Various |
| **Date of publication** | 2016 |

### 3.9.1 DESCRIPTION

*Untreated connected wastewater* measures the percentage of domestic wastewater that is connected through a sewerage system and not treated to at least a primary treatment level. Wastewater discharge without adequate treatment could expose water bodies, the general public, and ecosystems to pollutants such as pathogens and nutrients. The indicator compounds two crucial elements of wastewater management: connection and treatment. Low connection rates reflect households' lack of access to public sewerage systems; the absence of at least primary treatment reflects a country's lack of capacity (infrastructure, institutional knowledge) to treat wastewater. Together these factors can indicate the level of a country's current capacity to manage its domestic wastewater through two main pathways: extremely low connection rates (below 1 percent), and high connection rates with little treatment. **Higher values indicate higher percentages of point source wastewater discharged without treatment.**

### 3.9.2 CALCULATION

Sewerage connection and wastewater treatment data come from a white paper published by the International Food Policy Research Institute (IFPRI) and Veolia (Xie et al. 2016). In brief, Xie et al. aggregate three of the leading research papers on country-level connection and treatment rates into one data set through a hierarchical methodology. The data include the percentage of households connected to sewerage systems (*percent connected),* and the percentage of wastewater connected left untreated (i.e., not treated using primary, secondary, or tertiary treatments) (*percent untreated*).

The calculation is based on the Environmental Performance Index's Wastewater Treatment (WWT) indicator (Wendling et al. 2018):

$$WWT = percent\ treated\ to\ at\ least\ primary \cdot percent\ connected$$

WWT examines the performance of wastewater treatment (Wendling et al. 2018). The untreated, connected wastewater indicator reverses the WWT to instead examine the hazard:

$$UCW = \begin{cases} -1, & c \leq 1\% \\ 100\% - \left((100\% - u) \cdot c\right), & otherwise \end{cases}$$

**IN WHICH,**

*UCW* | Unimproved/connected wastewater raw value in [%]

*c* | Percent connected wastewater in [%]

*u* | Percent untreated wastewater in [%]

### 3.9.3 CONVERSION TO RISK CATEGORIES

The risk thresholds are based on quantiles, with the exception of the "low to no wastewater connected" threshold. All data marked in this category are given the highest risk score and removed from the rest of the data set before the quantiles are calculated.

| RAW VALUE | RISK CATEGORY | SCORE |
|---|---|---|
| <30% | Low | 0–1 |
| 30–60% | Low–medium | 1–2 |
| 60–90% | Medium–high | 2–3 |
| 90–100% | High | 3–4 |
| 100% | Extremely high | 4–5 |
| | Low to no wastewater connected | 5 |

The raw values are remapped to a 0–5 scale using the following equation:

$$score = \begin{cases} 5, & r < 0\% \\ \frac{r-0}{30\%-0}, & r \leq 30\% \\ \frac{r-30\%}{60\%-30\%} + 1, & 30\% < r \leq 60\% \\ \frac{r-60\%}{90\%-60\%} + 2, & 60\% < r \leq 90\% \\ \frac{r-90\%}{99\%-90\%} + 3, & 90\% < r < 100\% \\ 5, & r = 100\% \end{cases}$$

Where *r* is the raw indicator value and *score* is the indicator score [0–5].

### 3.9.4 LIMITATIONS

Important sources of water pollution, such as industrial waste and agricultural runoff, are not included. Wastewater that may be treated on-site, such as with private septic tanks, is also not captured due to a lack of available data. In addition, the severity of water pollution, which depends on the magnitude of loadings of pollutants and dilution capacity of receiving water bodies, is not represented (from a 2017 personal communication with Xie). This indicator also does not account for all water pollution sources, as it is focused primarily on household connection rates.

## 3.10 Coastal Eutrophication Potential

| GENERAL: | |
|---|---|
| **Name** | Coastal Eutrophication Potential |
| **Subgroup** | Physical risk quality |
| **Risk element** | |


| RESULTS: | |
|---|---|
| **Spatial resolution** | Hydrological sub-basin (HydroBASINS 6) |
| **Temporal resolution** | Annual baseline |

| SOURCE: | |
|---|---|
| **Spatial resolution** | Simulated Topological Network (STN) |
| **Temporal resolution** | Annual |
| **Temporal range** | 2000 |

| EXTRA: | |
|---|---|
| **Partner organization(s)** | Utrecht University, Washington State University |
| **Date of publication** | 2016 |

| ADDITIONAL DATA SOURCE | INPUT SPATIAL RESOLUTION | INPUT TEMPORAL RESOLUTION | INPUT TEMPORAL RANGE | SOURCE |
|---|---|---|---|---|
| STN Basins | 30 x 30 arc seconds | Annual | 2000 | Vörösmarty et al. (2000) |

### 3.10.1 DESCRIPTION

*Coastal eutrophication potential* (CEP) measures the potential for riverine loadings of nitrogen (N), phosphorus (P), and silica (Si) to stimulate harmful algal blooms in coastal waters. The CEP indicator is a useful metric to map where anthropogenic activities produce enough point-source and nonpoint-source pollution to potentially degrade the environment. When N and P are discharged in excess over Si with respect to diatoms, a major type of algae, undesirable algal species often develop. The stimulation of algae leading to large blooms may in turn result in eutrophication and hypoxia (excessive biological growth and decomposition that reduces oxygen available to other organisms). It is therefore possible to assess the potential for coastal eutrophication from a river's N, P, and Si loading. **Higher values indicate higher levels of excess nutrients with respect to silica, creating more favorable conditions for harmful algal growth and eutrophication in coastal waters downstream.**

### 3.10.2 CALCULATION

The calculation described below is based on Billen and Garnier's (2007) Indicator of Coastal Eutrophication Potential (ICEP) methodology. The nutrient data come from Bouwman et al. (2015). In short, the data are based on the Global NEWS 2 model (Mayorga et al. 2010) and aligned to Simulated Topological Network basins (Vörösmarty et al. 2000). The NEWS 2 model uses biophysical, natural, and anthropogenic (both point and nonpoint) nutrient sources, along with in-watershed and in-river removal processes, to derive global nutrient yields (Mayorga et al. 2010). Total N and P fluxes are calculated by summing NEWS 2 nutrient yield data for dissolved organic, dissolved inorganic, and particulate nutrients. Si fluxes are simply the dissolved inorganic Si yields in the basin.

The calculation is based on the Redfield molar ratio (C:N:P:Si = 106:16:1:20), which is a representation of the approximate nutrient requirement of marine diatoms (Billen and Garnier 2007):

$$CEP = \begin{cases} \left(\frac{j_N}{N \cdot 16} - \frac{j_{Si}}{Si \cdot 20}\right) \cdot 106 \cdot \frac{12}{365}, & if \frac{j_N}{N \cdot 16} > \frac{j_P}{P \cdot 1} \\ \left(\frac{j_P}{P \cdot 1} - \frac{j_{Si}}{Si \cdot 20}\right) \cdot 106 \cdot \frac{12}{365}, & otherwise \end{cases}$$

**IN WHICH,**

*CEP* | Coastal eutrophication potential [kg C-equivalent/km$^2$/day]

$j_n$ | Mean flux of total nitrogen delivered at the outlet of the river basin [kg N/km$^2$/yr]

$j_p$ | Mean flux of total phosphorus delivered at the outlet of the river basin [kg P/km$^2$/yr]

$j_{Si}$ | Mean flux of dissolved silica delivered at the outlet of the river basin[(kg Si/km$^2$/yr]

*N* | Molar mass of nitrogen [14g/mol]

*Si* | Molar mass of silica [28g/mol]

*P* | Molar mass of phosphrous [31g/mol]

A negative value indicates that silica is present in excess over the limiting nutrient and thus suggests the absence of eutrophication. A positive value indicates an excess of nutrients over the potential for diatom growth, suggesting suitable conditions for the growth of harmful algae (Garnier et al. 2010).

As a final step, the results are aggregated to HydroBASIN level 6 to align the indicator with the remainder of the framework.

### 3.10.3 CONVERSION TO RISK CATEGORIES

The thresholds used to convert raw values into risk scores are based on the suggested risk categories of the Transboundary Water Assessment Programme (TWAP) for ICEP (IOC-UNESCO and UNEP 2016), with one adjustment: the boundary between TWAP's low and medium categories was increased from -1 to 0 to better reflect the elevated risk warning in Aqueduct.

| RAW VALUE | RISK CATEGORY | SCORE |
|---|---|---|
| <-5 | Low | 0–1 |
| -5–0 | Low–medium | 1–2 |
| 0–1 | Medium–high | 2–3 |
| 1–5 | High | 3–4 |
| >5 | Extremely high | 4–5 |

The raw values are remapped to a 0–5 scale using the following equation:

$$score = \begin{cases} \frac{r - min(r_{all})}{-5 - min(r_{all})}, & r \leq -5 \\ \frac{r - -5}{0 - -5} + 1, & -5 < r \leq 0 \\ \frac{r - 0}{1 - 0} + 2, & 0 < r \leq 1 \\ \frac{r - 1}{5 - 1} + 3, & 1 < r \leq 5 \\ \frac{r - 5}{max(r_{all}) - 5} + 4, & r > 5 \end{cases}$$

Where *r* is the raw indicator value and *score* is the indicator score [0–5].

### 3.10.4 LIMITATIONS

Eutrophication can also impact freshwater, but a global data set for freshwater eutrophication potential is not currently available. Therefore, the indicator does not reflect the risk of eutrophication upstream of the coastal zone. In addition, the index calculation does not account for shifts in seasonality or the characteristics of the receiving water body.

## 3.11 Unimproved/No Drinking Water

| GENERAL: | |
|---|---|
| **Name** | Unimproved/No Drinking Water |
| **Subgroup** | Regulatory and reputational risk |
| **Risk element** | |


| RESULTS: | |
|---|---|
| **Spatial resolution** | Hydrological sub-basin (HydroBASINS 6) |
| **Temporal resolution** | Annual baseline |

| SOURCE: | |
|---|---|
| **Spatial resolution** | Country (rural/urban) |
| **Temporal resolution** | Annual |
| **Temporal range** | 2015 |

| EXTRA: | |
|---|---|
| **Partner organization(s)** | JMP |
| **Date of publication** | 2017 |

| ADDITIONAL DATA SOURCE | INPUT SPATIAL RESOLUTION | INPUT TEMPORAL RESOLUTION | INPUT TEMPORAL RANGE | SOURCE |
|---|---|---|---|---|
| Urban Extents | 30 arc seconds | Annual | 2010 | van Huijstee et al. (2018) |
| Gridded Population | 30 arc seconds | Annual | 2010 | van Vuuren et al. (2007) |

### 3.11.1 DESCRIPTION

*Unimproved/no drinking water* reflects the percentage of the population collecting drinking water from an unprotected dug well or spring, or directly from a river, dam, lake, pond, stream, canal, or irrigation canal (WHO and UNICEF 2017). Specifically, the indicator aligns with the *unimproved and surface water* categories of the Joint Monitoring Programme (JMP)—the lowest tiers of drinking water services. **Higher values indicate areas where people have less access to safe drinking water supplies.**

### 3.11.2 CALCULATION

Data for this indicator come from the 2015 drinking water access rates published by JMP (WHO and UNICEF 2017). The statistics from JMP's "at least basic" and "limited" fields are summed to represent the percentage of the population with access to *improved* drinking water. The *improved* rate is then inverted into the *unimproved/no access* rate by subtracting *improved* from 100 percent. This is done for the national, rural, and urban averages in each country. The national average is used to fill in any missing rural or urban averages.

The *unimproved/no access rate* is matched to each Aqueduct geometry (intersect of states, HydroBASIN 6, and aquifers; see 4.1) using the International Organization for Standardization (ISO) codes provided by the Database of Global Administrative Areas (GADM) ("GADM Metadata" n.d.).

*Rural and urban populations* are calculated for each Aqueduct geometry. Rural and urban populations come from a gridded 2010 population data set produced by the Netherlands Environmental Assessment Agency (PBL) (van Vuuren et al. 2007). The gridded population data set is parsed into rural and urban populations using a 2010 urban extent data layer (van Huijstee et al. 2018) and then summed by Aqueduct geometry.

The rural and urban *unimproved/no access rate* is multiplied by the *rural* and *urban populations*, respectively, to find the *number of people with unimproved/no access* to drinking water in each Aqueduct geometry. The rural and urban totals are then summed and aggregated to the HydroBASIN 6 scale, along with *total population*. Finally, the raw score—the *weighted percentage of population with unimproved/no access* per HydroBASIN 6—is calculated:

$$UDW = \frac{\sum_{basin}(r_{rural} \cdot pop_{rural} + r_{urban} \cdot \mathrm{pop}_{urban})}{\sum_{basin}(pop_{tot})}$$

**IN WHICH,**

*UDW* | Unimproved/no drinking water raw value in [-]

$r_{rural}$ | Rural unimproved/no access to drinking water rate in [-]

$r_{urban}$ | Urban unimproved/no access to drinking water rate in [-]

$pop_{rural}$ | Rural population in [number of people]

$pop_{urban}$ | Urban population in [number of people]

$pop_{tot}$ | Total population in [number of people]

### 3.11.3 CONVERSION TO RISK CATEGORIES

The risk thresholds are based on Aqueduct 2.1 (Gassert et al. 2014).

| RAW VALUE | RISK CATEGORY | SCORE |
|---|---|---|
| <2.5% | Low | 0–1 |
| 2.5–5.0% | Low–medium | 1–2 |
| 5.0–10.0% | Medium–high | 2–3 |
| 10.0–20.0% | High | 3–4 |
| >20.0% | Extremely high | 4–5 |

The raw values are remapped to a 0–5 scale using the following equation:

$$score = \max\left(0, min\left(\frac{ln(r) - ln(0.025)}{ln(2)}\right) + 1\right)$$

Where *r* is the raw indicator value and *score* is the indicator score [0–5].

### 3.11.4 LIMITATIONS

The unimproved/no drinking water indicator is presented at a finer resolution than originally published by JMP under the assumption that access rates among rural and urban communities are consistent throughout a country. The methodology fails to account for regional and local differences in access within countries.

## 3.12 Unimproved/No Sanitation

| GENERAL: | |
|---|---|
| **Name** | Unimproved/No Drinking Water |
| **Subgroup** | Regulatory and reputational risk |
| **Risk element** | |


| RESULTS: | |
|---|---|
| **Spatial resolution** | Hydrological sub-basin (HydroBASINS 6) |
| **Temporal resolution** | Annual baseline |

| SOURCE: | |
|---|---|
| **Spatial resolution** | Country (rural/urban) |
| **Temporal resolution** | Annual |
| **Temporal range** | 2015 |

| EXTRA: | |
|---|---|
| **Partner organization(s)** | JMP |
| **Date of publication** | 2017 |

| ADDITIONAL DATA SOURCE | INPUT SPATIAL RESOLUTION | INPUT TEMPORAL RESOLUTION | INPUT TEMPORAL RANGE | SOURCE |
|---|---|---|---|---|
| Urban Extents | 30 arc seconds | Annual | 2010 | van Huijstee et al. (2018) |
| Gridded Population | 30 arc seconds | Annual | 2010 | van Vuuren et al. (2007) |

### 3.12.1 DESCRIPTION

*Unimproved/no sanitation* reflects the percentage of the population using pit latrines without a slab or platform, hanging/bucket latrines, or directly disposing human waste in fields, forests, bushes, open bodies of water, beaches, other open spaces, or with solid waste (WHO and UNICEF 2017). Specifically, the indicator aligns with JMP's *unimproved and open defecation categories—the lowest tier of sanitation services*. **Higher values indicate areas where people have less access to improved sanitation services.**

### 3.12.2 CALCULATION

Data for this indicator come from the 2015 sanitation access rates published by JMP (WHO and UNICEF 2017). Statistics from JMP's "at least basic" and "limited" fields are summed to represent the percentage of the population with access to improved sanitation. The improved rate is then inverted into the unimproved/no access rate by subtracting improved from 100 percent. This is done for the national, rural, and urban averages in each country. The national average is used to fill in any missing rural or urban averages.

The unimproved/no access rate is matched to each Aqueduct geometry (intersect of states, HydroBASINS 6, and aquifers; see 4.1) using the International Organization for Standardization (ISO) codes provided by GADM ("GADM Metadata" n.d.).

Rural and urban populations are calculated for each Aqueduct geometry. Rural and urban populations come from a gridded 2010 population data set produced by PBL (van Vuuren et al. 2007). The gridded population data set is parsed into rural and urban populations using a 2010 urban extent data layer (van Huijstee et al. 2018), and then summed by Aqueduct geometry.

The rural and urban *unimproved/no access rate* is multiplied by the *rural and urban populations,* respectively, to find the number of people with *unimproved/no access* to sanitation in each Aqueduct geometry. The rural and urban totals are then summed and aggregated to the HydroBASINS 6 scale, along with *total population*. Finally, the raw score—*the weighted percentage of population with unimproved/no access* per HydroBASINS 6—is calculated:

$$USA = \frac{\sum_{basin}(r_{rural} \cdot pop_{rural} + r_{urban} \cdot \mathrm{pop}_{urban})}{\sum_{basin}(pop_{tot})}$$

**IN WHICH,**

*USA* | Unimproved/no sanitation raw value in [-]

$r_{rural}$ | Rural unimproved/no access to sanitation rate in [-]

$r_{urban}$ | Urban unimproved/no access to sanitation rate in [-]

$pop_{rural}$ | Rural population in [number of people]

$pop_{urban}$ | Urban population in [number of people]

$pop_{tot}$ | Total population in [number of people]

### 3.12.3 CONVERSION TO RISK CATEGORIES

The risk thresholds are based on Aqueduct 2.1 (Gassert et al. 2014).

| RAW VALUE | RISK CATEGORY | SCORE |
|---|---|---|
| <2.5% | Low | 0–1 |
| 2.5–5.0% | Low–medium | 1–2 |
| 5.0–10.0% | Medium–high | 2–3 |
| 10.0–20.0% | High | 3–4 |
| >20.0% | Extremely high | 4–5 |

The raw values are remapped to a 0–5 scale using the following equation:

$$score = \max\left(0, min\left(\frac{ln(r) - ln(0.025)}{ln(2)}\right) + 1\right)$$

Where *r* is the raw indicator value and *score* is the indicator score [0–5].

### 3.12.4 LIMITATIONS

Unimproved/no sanitation is presented at a finer resolution than is originally published by JMP under the assumption that access rates among rural and urban communities are consistent throughout a country. The methodology fails to account for regional and local differences in access within countries.

## 3.13 Peak RepRisk Country ESG Risk Index

| GENERAL: | |
|---|---|
| **Name** | Peak RepRisk Country ESG Risk Index |
| **Subgroup** | Regulatory and reputational risk |
| **Risk element** | |


| RESULTS: | |
|---|---|
| **Spatial resolution** | Country |
| **Temporal resolution** | Annual baseline |

| SOURCE: | |
|---|---|
| **Spatial resolution** | Country |
| **Temporal resolution** | Annual |
| **Temporal range** | 2016–18 |

| EXTRA: | |
|---|---|
| **Partner organization(s)** | RepRisk |
| **Date of publication** | 2018 |

### 3.13.1 DESCRIPTION

The Peak RepRisk country ESG risk index quantifies business conduct risk exposure related to environmental, social, and governance (ESG) issues in the corresponding country. The index provides insights into potential financial, reputational, and compliance risks, such as human rights violations and environmental destruction. RepRisk is a leading business intelligence provider that specializes in ESG and business conduct risk research for companies, projects, sectors, countries, ESG issues, NGOs, and more, by leveraging artificial intelligence and human analysis in 20 languages. WRI has elected to include the Peak RepRisk country ESG risk index in Aqueduct to reflect the broader regulatory and reputational risks that may threaten water quantity, quality, and access. While the underlying algorithm is proprietary, we believe that our inclusion of the Peak RepRisk country ESG risk index, normally unavailable to the public, is a value-add to the Aqueduct community. The peak value equals the highest level of the index in a given country over the last two years. **The higher the value, the higher the risk exposure.**

### 3.13.2 CALCULATION

RepRisk screens over 80,000 media, stakeholder, and third-party sources daily to identify and analyze ESG-related risk incidents and quantify them into the Peak RepRisk country ESG risk index (RepRisk n.d.). The results of the screening process are delivered to the RepRisk team of analysts, who are responsible for curating and analyzing the information. They hand select the items, give each risk incident a score (based on severity, source, and novelty), and write a risk summary. Before the risk incident is published, a senior analyst runs a quality check to ensure that the process has been completed in line with RepRisk's strict, rules-based methodology. After the senior analyst has given her or his approval, the final step in the process, the quantification of the risk, is performed through data science. The Peak RepRisk country ESG risk index takes into consideration the impact of a country's risk incidents within the last two years and the average of a country's Worldwide Governance Indicators. The data used in Aqueduct 3.0 cover October 2016 through October 2018. To learn more about RepRisk, please visit https://www.reprisk.com/our-approach or contact RepRisk.

#### 3.13.3 CONVERSION TO RISK CATEGORIES

The risk thresholds are based on guidance from RepRisk (RepRisk n.d.).

| RAW VALUE | RISK CATEGORY | SCORE |
|---|---|---|
| <25% | Low | 0–1 |
| 25–50% | Low–medium | 1–2 |
| 50–60% | Medium–high | 2–3 |
| 60–75% | High | 3–4 |
| >75% | Extremely high | 4–5 |

The raw values are remapped to a 0–5 scale using the following equation:

$$score = \begin{cases} \frac{r}{25\%}, & r \leq 25\% \\ \frac{r-25\%}{50\%-25\%} + 1, & 25\% < r \leq 50\% \\ \frac{r-50\%}{60\%-50\%} + 2, & 50\% < r \leq 60\% \\ \frac{r-60\%}{75\%-60\%} + 3, & 60\% < r \leq 75\% \\ \frac{r-75\%}{100\%-75\%} + 4, & r > 75\% \end{cases}$$

Where *r* is the raw indicator value and *score* is the indicator score [0–5].

# 4. GROUPED AND OVERALL WATER RISK

After calculating the 13 indicators and converting them to a uniform 0–5 scale, we can calculate the grouped and overall water risks (composite indices). See Figure 1 for an overview of the groups.

## 4.1 Geometries

Each of the 13 indicators is calculated at one of three different spatial scales: hydrological sub-basin, country, or groundwater aquifer. See "results: spatial resolution" in the summary table of each indicator. To combine the indicators into one framework, we take the union of the three geometries. The resulting geometries are a unique combination of a hydrological basin, groundwater aquifers, and an administrative boundary.

## 4.2 Weighted Aggregation

The subgroups (physical risk quantity, physical risk quality, and regulatory and reputational risk) and overall risks are calculated by taking a weighted average of the indicators that belong to each subgroup.

Exposure to water-related risks varies with the characteristics of water users. To obtain aggregated water risk scores, users can modify the weight of each indicator to match their exposure to the different aspects of water risk. There are five weights, or descriptors of relevance, on a base 2 exponential scale. This is preferred over a linear scale because of the human tendency to categorize intensity by orders of magnitude of difference (Triantaphyllou 2010). Users can also exclude indicators completely from aggregation. See Table 2 for an overview of the weights.

Table 2 | **Industry or User Relevance Weights and Their Descriptions**

| LEGEND | WEIGHT | INTERPRETATION |
|---|---|---|
| No weight | 0 | Not relevant |
| Very low | 0.25 | Represents very low relevance to the industry or user |
| Low | 0.5 | Represents low relevance to the industry or user |
| Medium | 1 | Represents medium relevance to the industry or user |
| High | 2 | Represents high relevance to the industry or user |
| Very high | 4 | Represents very high relevance to the industry or user |

*Source:* WRI.

Users have three options for the weighting scheme: default, industry-specific, or custom.

### Default weighting scheme

To determine a default set of indicator weights, we used input from six staff water experts following the principles of the Delphi technique. This technique uses a series of intensive questionnaires interspersed with controlled opinion feedback to obtain the most reliable consensus of opinion from a group of experts (Rowe and Wright 1999). The Delphi technique is intended for use in judgment situations; that is, ones in which pure model-based statistical methods are not practical or possible because of the lack of appropriate historical data, and thus some form of human judgment input is necessary (Dalkey and Helmer 1963). The lack of consistent information on exposure to water risks and the subjective nature of indicator weights made this technique an ideal fit. The results of the default weighting scheme can be found in the first column of Table 3.

### Industry-specific weighting scheme

Additionally, we developed preset weighting schemes for nine industry sectors on the basis of information provided in corporate water disclosure reports and input from industry experts to reflect the risks and challenges faced by each water-intensive sector. For each industry, we modified the default indicator weights on the basis of the relative importance of each indicator to the industry using information disclosed by companies on their exposure to, and losses from, water-related risks. To validate the industry-sector preset weighting schemes, we presented preliminary weighting schemes to industry representatives from the nine sectors and solicited feedback on the relative importance of each indicator for their sector. The results can be found in Table 3.

### Custom weighting scheme

In the online tool, users can specify their own custom weighting scheme.

Using the weighting schemes, grouped water risk scores can be calculated. The relative weight of each indicator is illustrated in Figure 7. The definition for each subgroup is listed below:

### Physical Risk Quantity

Physical Risk Quantity measures risk related to too little or too much water by aggregating all selected indicators from the physical risk quantity category. Higher values indicate higher water quantity risks.

### Physical Risk Quality

Physical Risk Quality measures risk related to water that is unfit for use by aggregating all selected indicators from the Physical Risk Quality category. Higher values indicate higher water quality risks.

### Regulatory and Reputational Risk

Regulatory and Reputational Risk measures risk related to uncertainty in regulatory change, as well as conflicts with the public regarding water issues. Higher values indicate higher regulatory and reputational water risks.

Finally, the three grouped water risk scores can be used to determine the overall water risk score. The sums of the weights are used to calculate the relative contribution of each group.

### Overall Water Risk

Overall Water Risk measures all water-related risks, by aggregating all selected indicators from the Physical Risk Quantity, Physical Risk Quality, and Regulatory and Reputational Risk categories. Higher values indicate higher water risk.

Table 3 | **Industry or User Relevance Weights and Their Descriptions**

| | | | Default | Agriculture | Chemicals | Construction Materials | Electric Power | Food and Beverage | Mining | Oil and Gas | Semiconductor | Textile |
|---|---|---|---|---|---|---|---|---|---|---|---|---|
| PHYSICAL RISK QUANTITY | 1 | Baseline water stress | 4 | 4 | 2 | 2 | 4 | 4 | 2 | 1 | 2 | 2 |
| | 2 | Baseline water depletion | 4 | 4 | 2 | 2 | 4 | 4 | 2 | 1 | 2 | 2 |
| | 3 | Interannual variability | 0.5 | 2 | 1 | 0.5 | 1 | 1 | 1 | 0.5 | 1 | 1 |
| | 4 | Seasonal variability | 0.5 | 0.5 | 1 | 0.5 | 2 | 0.5 | 1 | 0.5 | 1 | 0.5 |
| | 5 | Groundwater table decline | 4 | 4 | 2 | 2 | 0.5 | 4 | 2 | 1 | 2 | 2 |
| | 6 | Riverine flood risk | 1 | 1 | 4 | 1 | 2 | 0.5 | 4 | 1 | 1 | 1 |
| | 7 | Coastal flood risk | 1 | 1 | 4 | 1 | 4 | 0.5 | 4 | 4 | 1 | 2 |
| | 8 | Drought risk | 2 | 4 | 2 | 1 | 4 | 2 | 4 | 0.5 | 1 | 1 |
| PHYSICAL RISK QUALITY | 9 | Untreated connected wastewater | 2 | 1 | 2 | 1 | 0.25 | 2 | 0.5 | 0.25 | 4 | 4 |
| | 10 | Coastal eutrophication potential | 1 | 4 | 0.25 | 0.5 | 1 | 2 | 0.25 | 0 | 2 | 1 |
| REGULATORY AND REPUTATIONAL RISK | 11 | Unimproved/no drinking water | 2 | 2 | 2 | 1 | 0.25 | 1 | 4 | 4 | 1 | 2 |
| | 12 | Unimproved/no sanitation | 2 | 2 | 2 | 1 | 0.25 | 1 | 4 | 4 | 1 | 2 |
| | 13 | Peak RepRisk country ESG risk index | 0.5 | 0.25 | 2 | 0.5 | 0.25 | 2 | 4 | 4 | 2 | 4 |

*Source:* WRI.

Figure 7 | **Indicator Weights per Industry**

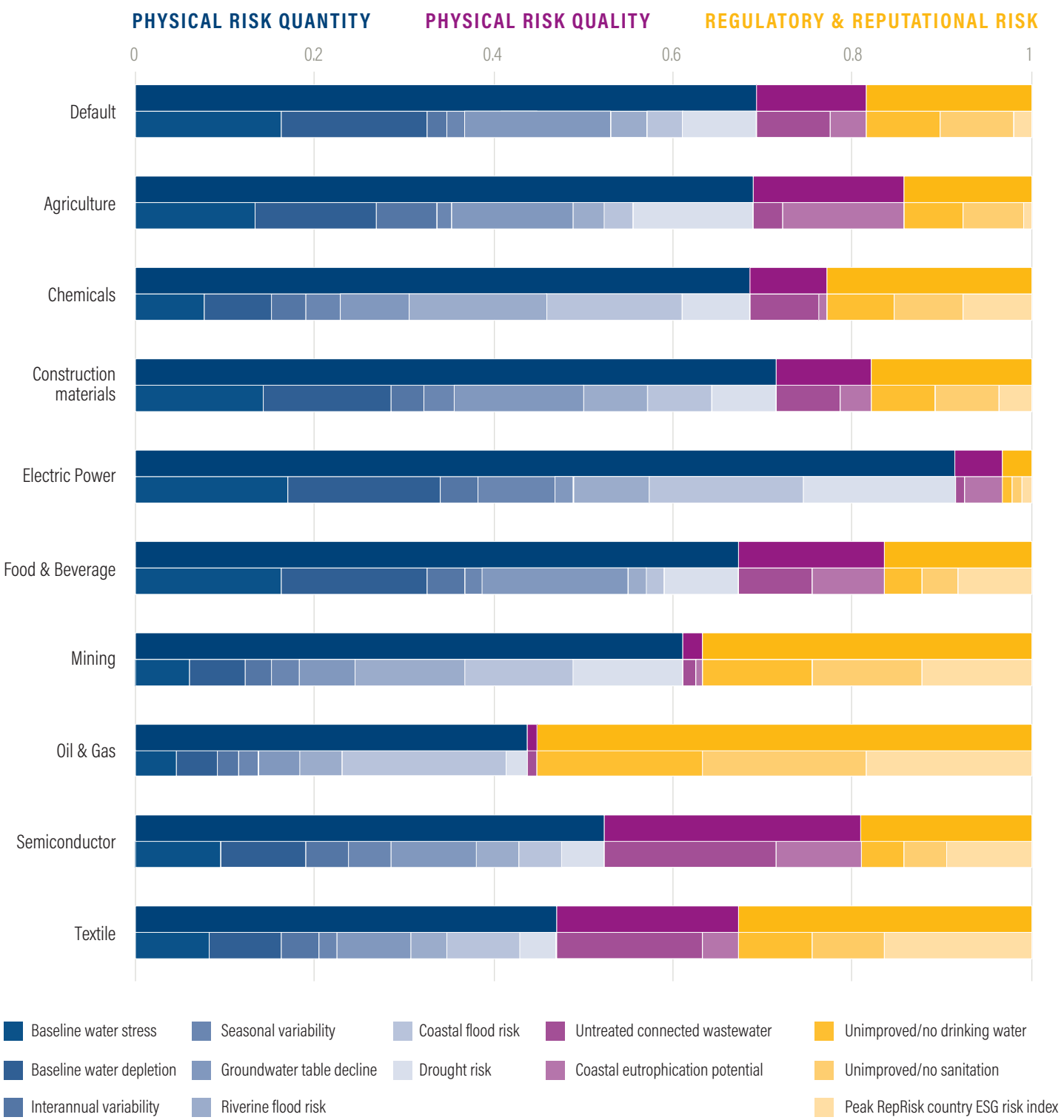


*Notes:* Weights are based on data availability. Masked or NoData values are excluded from the aggregated weighting. Please see the online tool for the results. The data are also available for download.
*Source:* WRI.

# 5. LIMITATIONS

Not every aspect of water risk has usable global data sets enabling it to be incorporated into our framework. Certain important elements are partially missing from the framework, such as water management and governance.[18]

The local social dimensions of water risks are not incorporated into this framework and database. Policy, regulation, and response to water crises are paramount in estimating water risks and fully understanding their impacts. In the end, each region or location's ability to cope with water-related issues will affect its water risk.

Several limitations are associated with the framework (composite index) approach. First, it requires mapping the indicators to comparable (0–5) scale, thereby losing information such as absolute values. The second limitation, linked to the first, is that we combined data with various spatial and temporal resolutions and ranges into a single framework. Third, there are only two and three indicators in the quality and regulatory and reputational groups respectively. This makes these groups sensitive to errors in the underlying data. We provide industry and custom weighting to mitigate this limitation, but this requires the user to understand the data. The framework's water quality indicators do not reflect the full range of water quality threats but focus on nutrient pollution. The framework does not endorse framing water-quality solutions solely around coastal eutrophication or municipal wastewater. A fourth limitation of the framework approach is the mixing of risk types. The framework is inconsistent in including the exposure and vulnerability layers for all indicators.

In addition to the limitations of the framework approach, each indicator comes with its own limitations. For the indicator-specific limitations, please see the indicator sections above and the associated literature. Since many of the indicators rely on the PCR-GLOBWB 2 hydrological model and HydroBASINS 6 (hydrological sub-basins), some of these specific limitations are copied below.

Coastal sub-basins and islands in HydroBASINS 6 are often grouped for various reasons explained in Lehner et al. (2008). This grouping is coarse and results in inaccuracies, primarily when water demand can be satisfied using remote water supply.

PCR-GLOBWB 2 has no means to model interbasin transfer. Interbasin transfer happens when demand in one sub-basin is satisfied with supply from another sub-basin that is not upstream. Many major metropolitan areas source their water from adjacent sub-basins. Thus, baseline water stress in a given sub-basin may at times appear worse than it is where interbasin transfers are available to meet demand in that catchment. Alternatives to the moving window size and regression method used to process the PCR-GLOBWB 2 results could not be assessed due to the lack of validation data.

Direct validation of the aggregated grouped water risks and overall water risk is not possible. The perception of water risk is subjective, and robust validation methods for multi-indicator frameworks are unavailable.

It is crucial to understand what the Aqueduct 3.0 framework and database can and cannot do. Like version 2.1, Aqueduct 3.0 is tailored to comparing regions on a larger scale. It has limited application at a local level. The presented results should therefore be used as a prioritization tool, after which deeper dive assessments should be used to understand local conditions with greater accuracy.

## APPENDIX A: DEMAND, WITHDRAWAL, AND RETURN FLOW

This appendix describes the hydrological terminology used in PCR-GLOBWB 2. An overview is shown in Figure A1. PCR-GLOBWB 2 determines water demand. Withdrawal is demand limited by available water.

Withdrawal consists of two components: Consumptive withdrawal and nonconsumptive withdrawal. Gross withdrawal refers to consumptive plus nonconsumptive withdrawal. Net withdrawal refers to only the consumptive withdrawal.

The nonconsumptive withdrawal will return to the water body, usually downstream, and is also referred to as return flow.

Figure A1 | **Schematic of Demand, Gross and Net Withdrawal, and Return Flow**

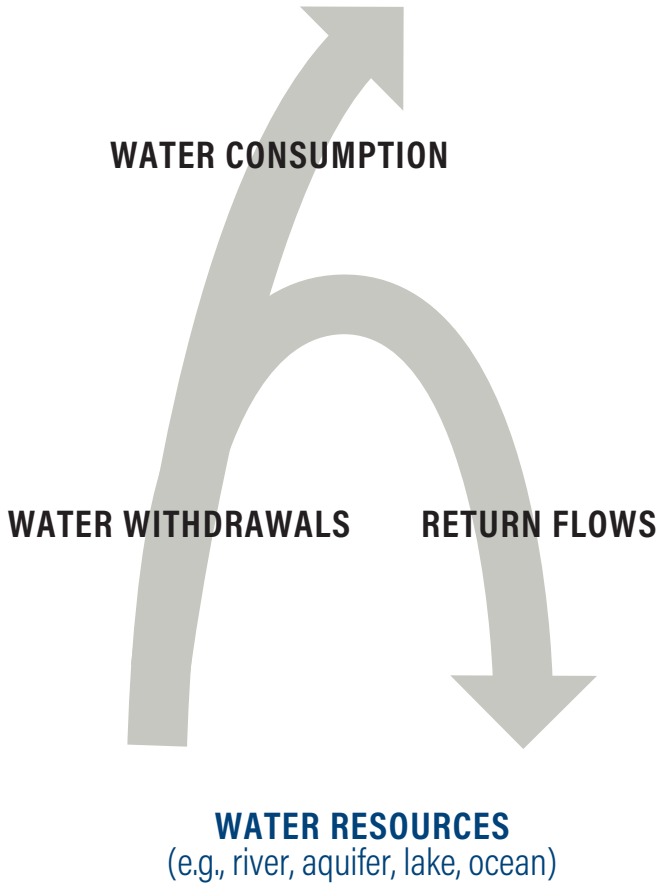


*Source:* WRI.

## APPENDIX B: GEOGRAPHIC CONVERSION TABLE

Table B1 is intended to provide a quick and approximate sense of scale.

Table B1 | **Common Arc Lengths**

| ARC LENGTH | DECIMAL DEGREES | DISTANCE AT EQUATOR (KM) | APPROXIMATE DISTANCE AT EQUATOR (KM) |
|---|---|---|---|
| 360 arc degrees | 360 | 40,030.17 | 40,000 |
| 1 arc degree | 1 | 111.19 | 110 |
| 30 arc minutes | 0.5 | 55.60 | 55 |
| 5 arc minutes | 0.08333 | 9.27 | 10 |
| 1 arc minute | 0.016667 | 1.85 | 2 |
| 30 arc seconds | 0.008333 | 0.93 | 1 |
| 15 arc seconds | 0.004167 | 0.46 | .5 |

*Source:* WRI.

# APPENDIX C: PCR-GLOBWB 2

Baseline water stress, baseline water depletion, interannual variability, seasonal variability, groundwater table decline, and elements of the flood risk indicators are all based on the PCRaster Global Water Balance 2 model (PCR-GLOBWB 2) (Sutanudjaja et al. 2018).

This appendix covers the basic model structure of PCR-GLOBWB 2 and the settings used for the Aqueduct run.

For baseline water stress, baseline water depletion, interannual variability, and seasonal variability we used a setup with default groundwater configuration. We will refer to this run as the default PCR-GLOBWB 2 run.

For the groundwater table decline indicator, we used a setup of PCR-GLOBWB 2 with an advanced representation of groundwater based on MODFLOW. We will refer to this setup as the PCR-GLOBWB 2 + MODFLOW run.

## Digital Elevation Model

The starting point of almost any hydrological model and analysis is a digital elevation model (DEM). The DEM will determine the runoff direction; that is, the way the water flows. Aqueduct uses the same DEM as PCR-GLOBWB 2 and is a combination of the 30 × 30 arc second HydroSheds data (Lehner et al. 2008) with GTOPO30 (Gesch et al. 1999) and Hydro1k (Verdin and Greenlee 1996). Lakes and wetlands from the Global Lakes and Wetlands Database (GLWD) (Lehner and Döll 2004a) are extracted. Finally, reservoirs and dams from the Global Reservoir and Dam (GRanD) database have been used (Lehner et al. 2011). The result is a hydrologically corrected data set of elevation, resampled to the PCR-GLOBWB resolution of 5 × 5 arc minutes (approximately 10 km at the equator).

## Local Drainage Direction

The local drainage direction, or the way water flows from one grid cell to the next, is derived from the DEM and assumes a strictly convergent flow. This means that in PCR-GLOBWB 2 and Aqueduct, bifurcations and river deltas are modeled as one stream instead of splitting rivers.

## Model Structure

PCR-GLOBWB 2 is a grid-based, modular global hydrological model. The world is represented by a 4,320 × 2,610 grid with a resolution of 5 × 5 arc minutes. For each of these cells, the model contains the following modules:

- Meteorological forcing
- Land surface
- Groundwater
- Surface water routing
- Irrigation and water use

See Figure C1 for a schematic representation of the model.

### Meteorological forcing module

To model key weather elements that affect hydrology, the meteorological forcing of PCR-GLOBWB 2 uses daily time series of spatial fields of precipitation, temperature, and reference evaporation.

The default run is forced using data from two data sources: WATCH for the period 1960–76 and WATCH Era Interim (WFDEI) to extend the analysis to 2014 (Weedon et al. 2014).

Reference evapotranspiration is calculated using Penman-Monteith, according to the FAO guidelines (Allen et al. 1998).

The PCR-GLOBWB 2 + MODFLOW run is forced using combined Climatic Research Unit (CRU) and Era-Interim (Harris et al. 2014; Dee et al. 2011). Although the model ran for 1959–2015, only the results for 1990–2014 have been used to calculate the groundwater table decline indicator (Verdin and Greenlee 1996).

#### LAND SURFACE MODULE

This is the central module of PCR-GLOBWB 2 and connects directly to all other modules. It consists of multiple vertically stacked layers: canopy, snow, soil layer 1 (S1), and soil layer 2 (S2). See Figure C1. There are vertical fluxes between the stacked layers (e.g., S1 to S2 and vice versa), as well as with the climate forcing module (e.g., precipitation and evaporation) and the groundwater module (e.g., S2 to groundwater). Furthermore, there are horizontal fluxes to the runoff module. Within each grid cell, subgrid variability is modeled using a land-use class approach. This means that each grid cell is assigned a fraction of four land-use classes:

- Tall natural vegetation
- Short natural and nonnatural (rainfed crops) vegetation
- Nonpaddy-irrigated crops
- Paddy-irrigated crops (e.g., wet rice)

For instance, a grid cell might consist of 20 percent tall natural vegetation, 25 percent short vegetation, 40 percent nonpaddy-irrigated crops, and 15 percent paddy-irrigated crops (total 100 percent). Soil and vegetation parameters are obtained for each class and for each grid cell. Hence the soil and vegetation conditions are spatially distributed.

The Global Land Cover Characteristics Data Base, version 2.0 ("GLCC 2.0" 2010) and land surface parameter data set (Hagemann 2002) are used to assign the four land-use classes to each 5 arc minute grid cell as well as obtain a few soil and vegetation parameters.

For each of the four land-use classes and for each soil layer (S1 and S2), the remaining soil parameters are defined using FAO's Digital Soil Map of the World (Nachtergaele et al. 2009) and the WISE data set on global soil properties (Batjes 2012).

Finally, additional monthly vegetation properties, including leaf area index (LAI) and crop factors, are derived from the MIRCA 2000 data set (Portmann et al. 2010) and the Global Crop Water Model (Siebert and Döll 2010).

For each of the four land-use classes, the following evaporative fluxes are defined:

- Interception evaporation
- Bare soil evaporation
- Snow sublimation
- Vegetation-specific transpiration

Figure C1 | **PCR-GLOBWB 2 Schematic Overview**

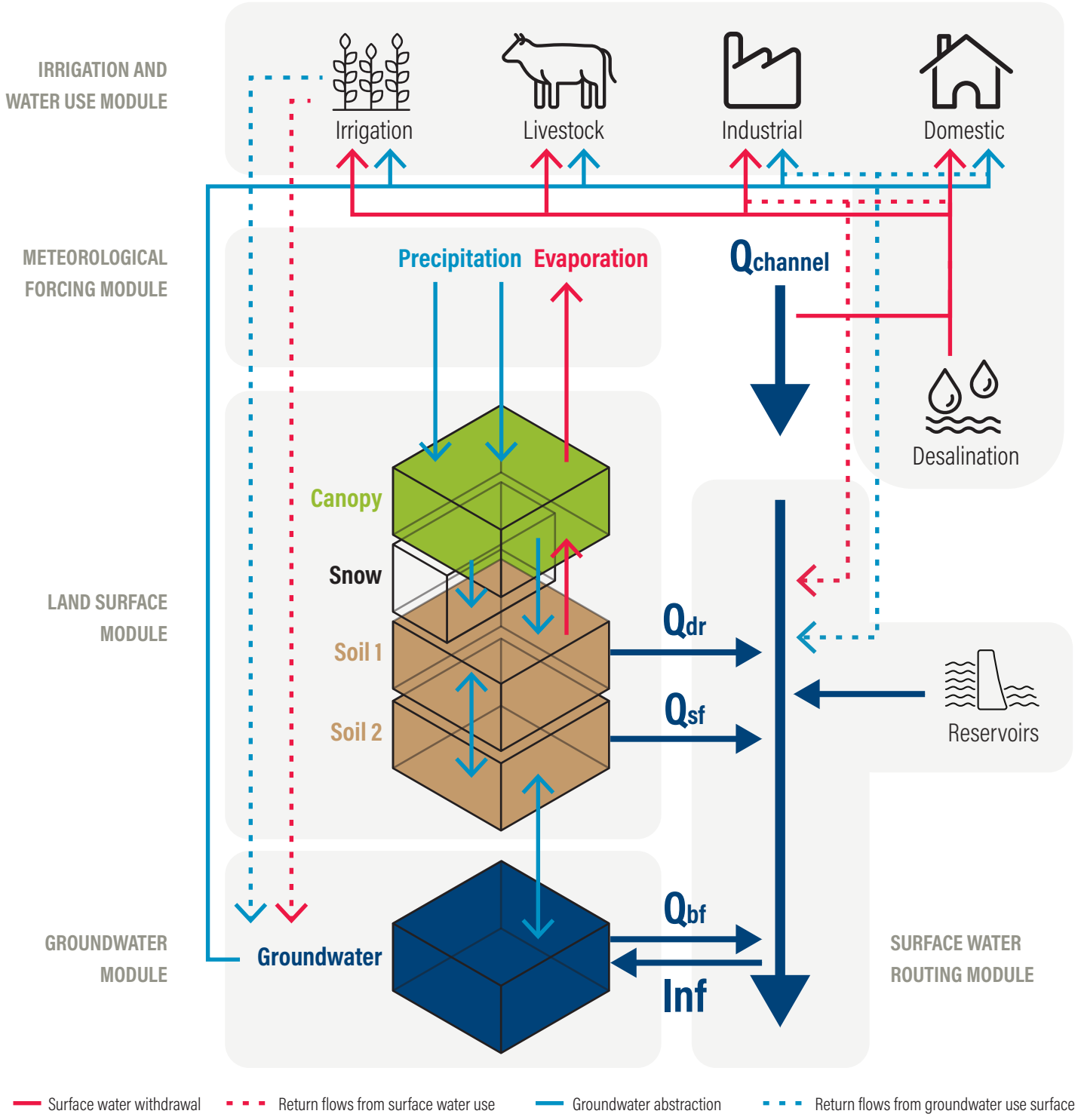


*Note:* "Schematic overview of a PCR-GLOBWB 2 cell and its modeled states and fluxes. S1, S2 (soil moisture storage), S3 (groundwater storage), Qdr (surface runoff—from rainfall and snowmelt), Qsf (interflow or stormflow), Qbf (baseflow or groundwater discharge), and Inf (riverbed infiltration from to groundwater). The thin red lines indicate surface water withdrawal, the thin blue lines groundwater abstraction, the thin red dashed lines return flows from surface water use, and the thin dashed blue lines return flows from groundwater use surface. For each sector, withdrawal – return flow = consumption. Water consumption adds to total evaporation. In the figure, the five modules that make up PCR-GLOBWB 2 are portrayed on the model components" (Sutanudjaja et al. 2018).
*Source:* Based on raw data from Sutanudjaja et al. (2018), modified/aggregated by WRI.

Another main building block in the land surface model is runoff and infiltration modeling. There are two runoff components in the land surface module: (1) direct runoff from soil layer 1 combined with snowmelt from the snow layer and (2) stormflow[19] runoff from soil layer 2.

Direct and stormflow runoff are determined by excess infiltration according to the advanced ARNO scheme approach (Todini 1996; Hagemann and Gates 2003). This scheme determines which fraction will transfer vertically (infiltration) or horizontally (runoff).

## Groundwater module

For the default setup, the groundwater module calculates groundwater storage dynamics subject to recharge and capillary rise (calculated by the land surface module), groundwater discharge ($Q_{bf}$) and riverbed infiltration (Inf). Groundwater discharge depends on a linear storage-outflow relationship ($Q_{bf} = S3/J$) in which the proportionality constant $J$ is calculated following Kraijenhoff van de Leur (1958). Riverbed infiltration occurs only in the case that $Q_{bf}$ becomes 0 by groundwater withdrawal. Under persistent groundwater withdrawal (calculated with the irrigation and water use module), the groundwater storage $S3$ is allowed to become negative. In this case, the part of the withdrawn groundwater in excess of the input (recharge and riverbed infiltration) is seen as nonrenewable groundwater withdrawal leading to groundwater depletion.

For the groundwater run, we use a groundwater flow model based on MODFLOW to simulate spatiotemporal groundwater heads (Harbaugh et al. 2000). This is a one-way coupling in which PCR-GLOBWB 2 is first run with the standard groundwater module (reservoir $S3$ with only vertical fluxes) to yield time series of net groundwater recharge (recharge – capillary rise) and surface water levels. These fluxes and inputs are subsequently used to force the groundwater flow model (see, e.g., Sutanudjaja et al. 2011; and de Graaf et al. 2015, 2017).

## Irrigation and water use module

Water demand and withdrawal are fully coupled, which means that demand and withdrawal influence the state of other model components and vice versa. PCR-GLOBWB 2 determines demand and withdrawal for four sectors: domestic, industrial, irrigation, and livestock. See Appendix A for a description of demand, withdrawal, and return flow.

For each sector, gross and net demand is calculated. Gross demand consists of consumptive and nonconsumptive demand, whereas net demand consists of only consumptive demand.

## Irrigation demand

Irrigation water demand is determined using monthly irrigated areas per grid cell, crop phenology, and crop factors, which are based on FAOSTAT, MIRCA 2000, and the Global Crop Water Model, respectively ("FAOSTAT" 2012; Portmann et al. 2010; Siebert and Döll 2010). Although the total irrigated area per cell varies over time, the ratio of paddy/nonpaddy irrigation is kept constant due to limitations in the input data.

The irrigation water requirements are derived from FAO guidelines (Allen et al. 1998; Doorenbos and Pruitt 1977). Paddy and nonpaddy crops are calculated separately and are both fully coupled with changes in surface and groundwater balance. Evapotranspiration is dynamically modeled using soil, vegetation, climate, and crop states. For more information, see Wada et al. (2014a).

The process is illustrated in Figure C2. Associated input data sets are shown in Table C1.

Figure C2 | **Irrigation Water Demand Schematic**

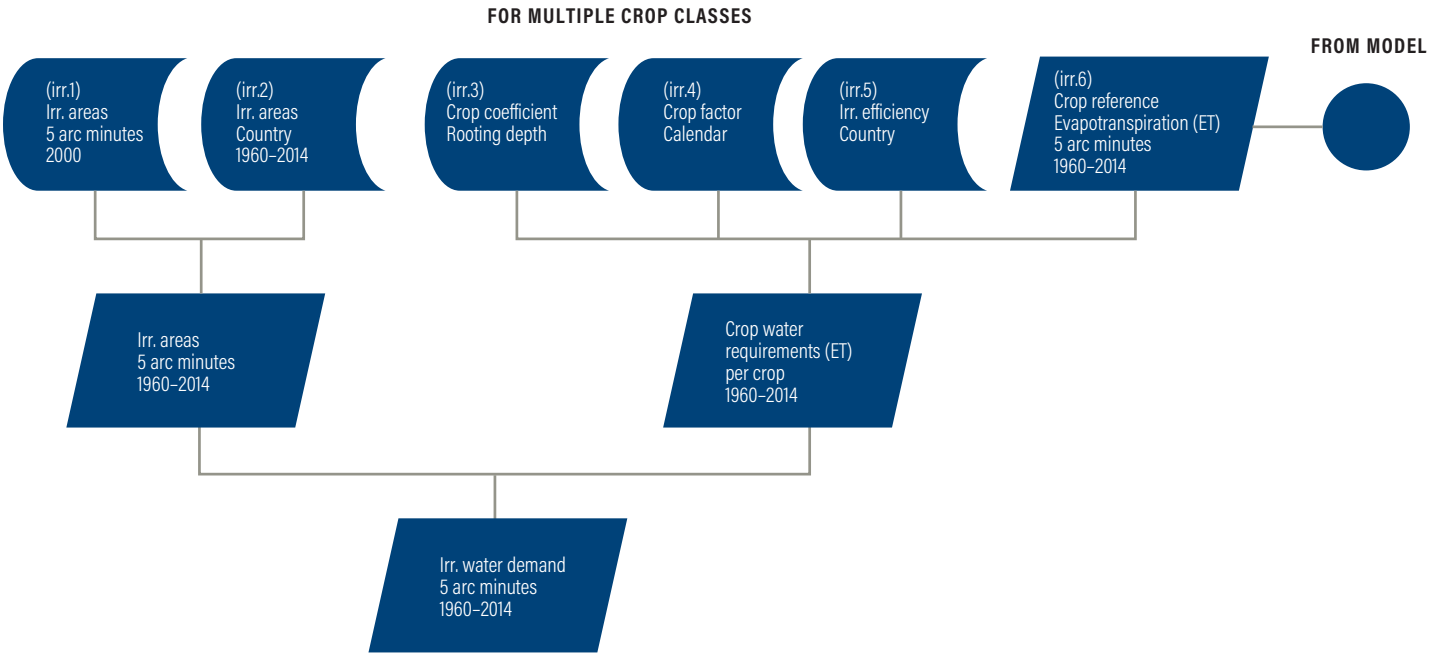


*Source:* Based on raw data from Wada et al. 2011a, modified/aggregated by WRI.

Table C1 | **Data Used to Determine Irrigation Water Demand in PCR-GLOBWB 2 run for Aqueduct 3.0**

| CODE | DESCRIPTION | INPUT SPATIAL RESOLUTION | INPUT TEMPORAL RESOLUTION | INPUT TEMPORAL RANGE | SOURCE |
|---|---|---|---|---|---|
| Irr.1 | Irrigated area | 5 arc minutes | Monthly | 2000 | MIRCA 2000 (Portmann et al. 2010) |
| Irr.2 | Historical growth of irrigated areas | Country | Annual | 1960–2014 | FAO ("FAOSTAT" 2012) |
| Irr.3 | Crop coefficient, rooting depth | N/A | N/A | N/A | Global Crop Water Model (Siebert and Döll 2010) |
| Irr.4 | Crop factor, crop calendar | 5 arc minutes | Monthly | 2000 | MIRCA 2000 (Portmann et al. 2010) |
| Irr.5 | Irrigation efficiency | Country | N/A | Various | Rohwer et al. (2007) |
| Irr.6 | Crop evapotranspiration | 5 arc minutes | Daily | 1960–2014 | From PCR-GLOBWB 2 model |

*Note:* The code corresponds to Figure C2.
*Source:* WRI.

## Industrial demand

Industrial demand captures water demand for manufacturing, power generation, and other industrial processes.

Before jumping into the calculation of industrial water demand, it is important to understand the definition of water use intensities. Water use intensities are used to derive time series (1960–2014) from a reference data set.

Water use intensities are calculated using four socioeconomic data sets:

- GDP
- Electricity production
- Energy consumption
- Household consumption

All data sets are annually per country for the period 1960–2014. The method to determine water use intensities from these data sets is explained in Wada et al. (2011a). The approach is depicted in Figure C3. The associated input data set appears in Table C2.

Figure C3 | **Water Use Intensities Schematic**

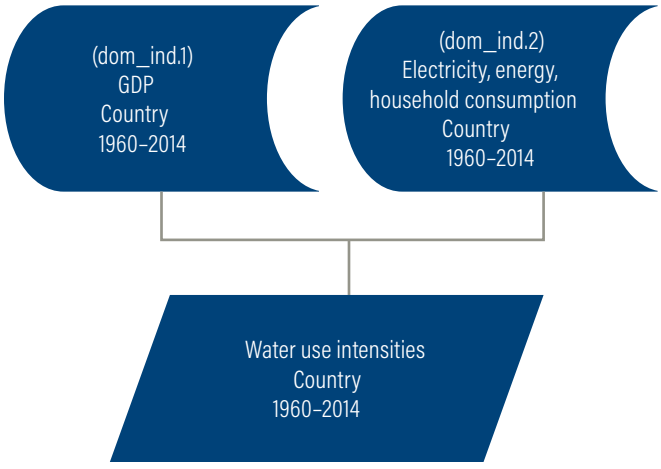


*Source:* Based on raw data from Wada et al. 2011a, modified/aggregated by WRI.

The water use intensities are then combined with a reference industrial water withdrawal data set to obtain time series (see Figure C4). The results are spatially disaggregated using nighttime lights to get gross industrial water demand at 5 arc minute resolution for the period 1960–2014. A precalculated recycle ratio per country, 1960–2014, based on the development of a country, is used to derive net industrial water demand from gross water demand. Industrial demand is assumed to be constant over a year due to data limitations.

## Table C2 | Data Used to Determine Water Use Intensities

| CODE | DESCRIPTION | INPUT SPATIAL RESOLUTION | INPUT TEMPORAL RESOLUTION | INPUT TEMPORAL RANGE | SOURCE |
|---|---|---|---|---|---|
| Dom_ind.1 | GDP | Country | Annual | 1960–2014 | World Bank (n.d.) |
| Dom_ind.2 | Electricity production, energy consumption, and household consumption | Country | Annual | 1960–2014 | UNEP (n.d.) |

*Note:* The code corresponds to Figure C3.
*Source:* Wada et al. 2011a.

## Figure C4 | Industrial Water Demand Schematic

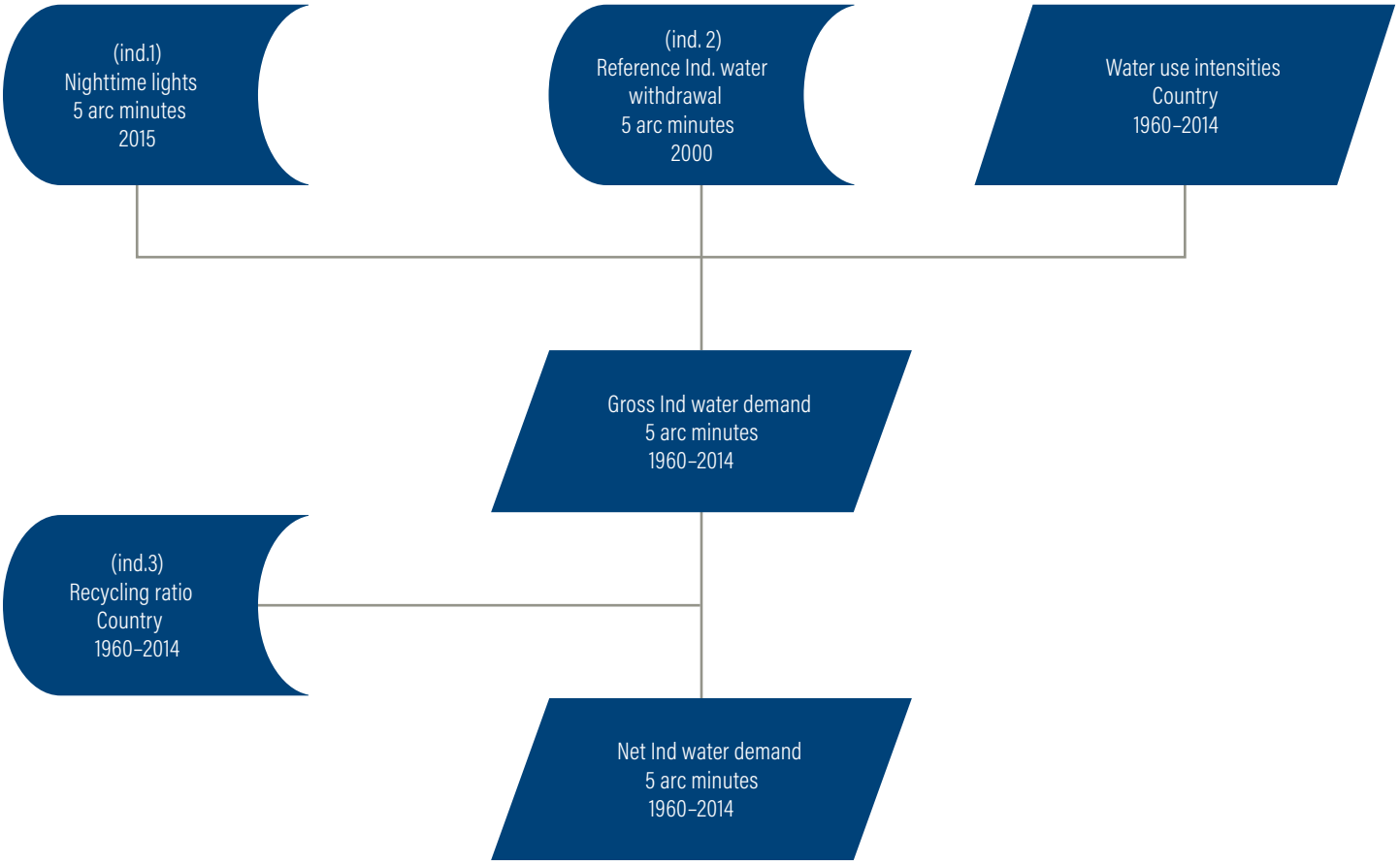


*Note:* Water use intensities are calculated in the previous step. The associated data sets can be found in Table C3.
*Source:* Based on raw data from Wada et al. 2011a, modified/aggregated by WRI.

## Livestock demand

Daily livestock demand is determined by multiplying the total number of livestock per grid cell by a corresponding daily drinking water requirement depending on temperature. Gridded livestock density for 1960–2014 is obtained by combining the gridded livestock densities of 2000 with historical livestock growth (see Figure C5). See Wada et al. (2014a) for full details.

### Table C3 | Data Used for Industrial Water Demand

| CODE | DESCRIPTION | INPUT SPATIAL RESOLUTION | INPUT TEMPORAL RESOLUTION | INPUT TEMPORAL RANGE | SOURCE |
|---|---|---|---|---|---|
| Ind.1 | Nighttime lights | 0.01 arc degree | Annual | 2015 | EOG and NOAA (n.d.) |
| Ind.2 | Reference industrial water withdrawal | 5 arc minutes | Annual | 2000 | WWDR-II data set (Shiklomanov 1997; WRI et al. 1998; Vörösmarty et al. 2005) |
| Ind.3 | Recycling ratio | Country | Annual | 1960–2014 | Wada et al. (2011a) |

*Note:* The code corresponds to Figure C4.
*Source:* WRI.

### Figure C5 | Livestock Water Demand Schematic

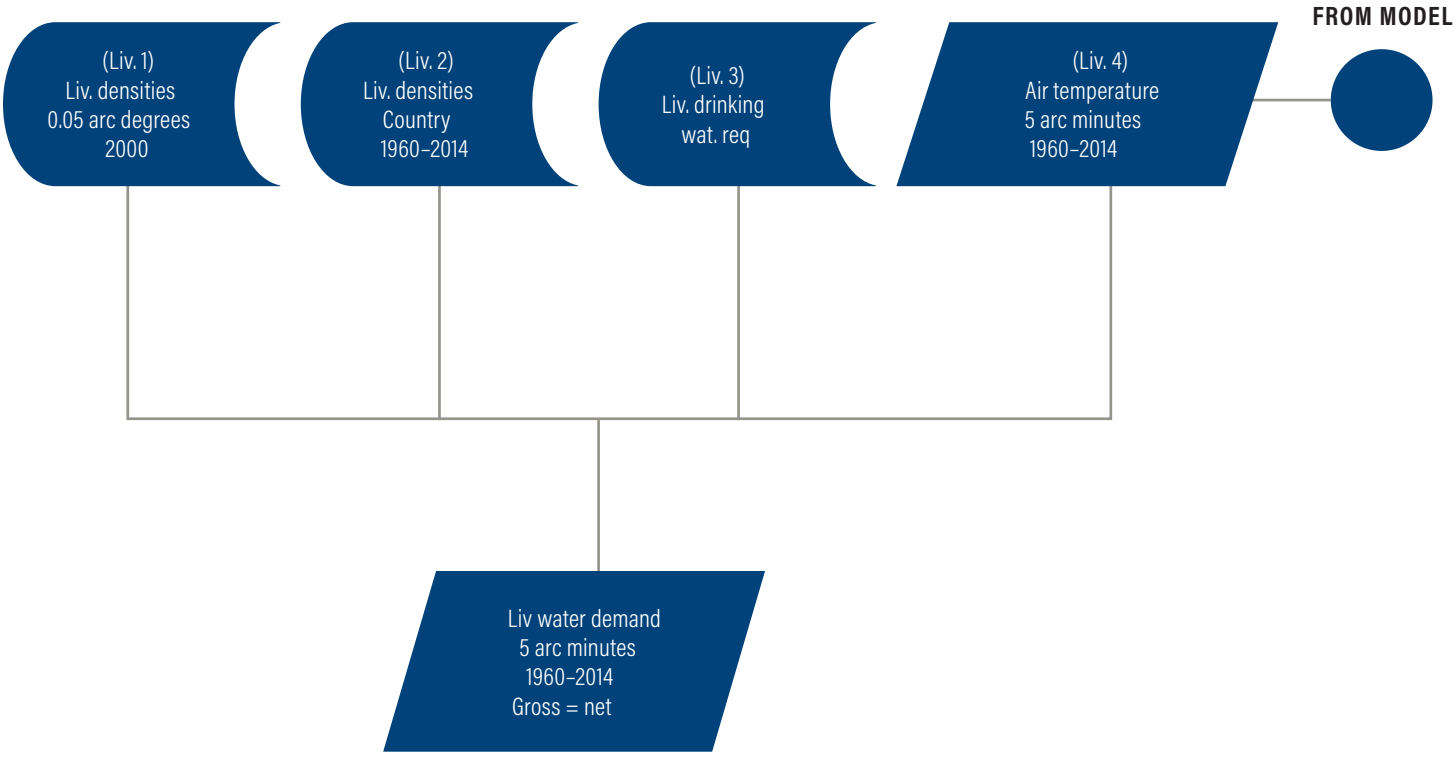


*Note:* The associated input data sets can be found in Table C4.
*Source:* Based on raw data from Wada et al. 2011a, modified/aggregated by WRI.

## Domestic demand

Domestic demand includes water demand from households in both urban and rural areas. Domestic water demand per country 1960–2014 is calculated by combining the total country population 1960–2014 with the average per capita water use of a reference year. The reference data are turned into a time series by temporarily disaggregating using the water use intensities data. The water use intensities are the same as used for industrial demand and explained in the "Industrial demand" section above.

Annual country demand data are then further processed using two other data sets: (1) gridded population and (2) gridded air temperature. The result is gross water demand at 5 × 5 arc minute resolution, daily 1960–2014. Domestic demand is modeled as a function of daily air temperature.

Net domestic demand is calculated by combining the gross demand with country-specific recycle ratios and with rural and urban access to water data (Figure C6). For more details, see Wada et al. (2011a).

Table C4 | **Data Used to Determine Livestock Water Demand in PCR-GLOBWB 2 Run for Aqueduct 3.0**

| CODE | DESCRIPTION | INPUT SPATIAL RESOLUTION | INPUT TEMPORAL RESOLUTION | INPUT TEMPORAL RANGE | SOURCE |
|---|---|---|---|---|---|
| Liv.1 | Gridded global livestock density for cattle, buffalo, sheep, goats, pigs, and poultry | 0.05 arc degrees | Annual | 2000 | FAO (Wint and Robinson 2007) |
| Liv.2 | Historical growth of livestock | Country | Annual | 1960–2014 | FAO ("FAOSTAT" 2012) |
| Liv.3 | Daily drinking water requirements | N/A | N/A | N/A | Steinfeld et al. 2006 |
| Liv.4 | Air temperature | 5 arc minutes | Daily | 1960–2014 | From climate forcing, meteorological forcing module |

*Note:* The code corresponds to Figure C5.
*Source:* WRI.

Figure C6 | **Domestic Demand Schematic**

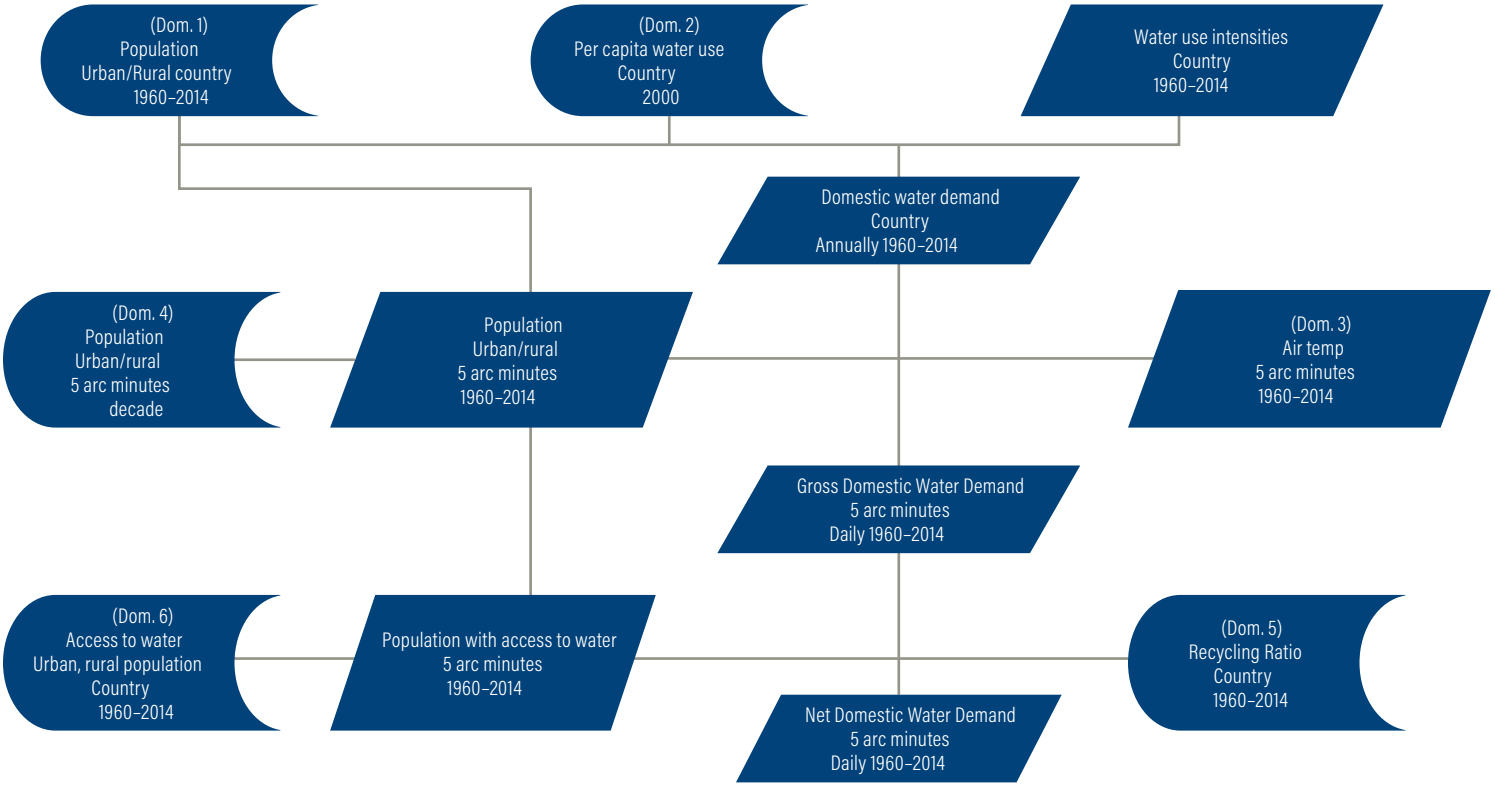


*Note:* The associated data sets can be found in Table C5.
*Source:* Based on raw data from Wada et al. 2011a, modified/aggregated by WRI.

Table C5 | **Data Used to Determine Domestic Water Demand**

| CODE | DESCRIPTION | INPUT SPATIAL RESOLUTION | INPUT TEMPORAL RESOLUTION | INPUT TEMPORAL RANGE | SOURCE |
|---|---|---|---|---|---|
| Dom.1 | Population | Country | Annual | 1960–2014 | FAO ("FAOSTAT" 2012) |
| Dom.2 | Per capita water use | Country | Annual | 2000 | FAO ("AQUASTAT," n.d.) |
| Dom.3 | Air temperature | 5 arc minutes | Daily | 1960–2014 | From PCR-GLOBWB 2 model |
| Dom.4 | Population, urban, rural | 5 arc minutes | Decadal, interpolated | 1960–2014 | IMAGE / HYDE (Bouwman et al. 2006) |
| Dom.5 | Recycling ratio | Country | Annual | 1960–2014 | Wada et al. (2011a) |
| Dom.6 | Access to water for urban and rural | Country | Annual | 1960–2014 | UNEP (n.d.) |

*Note:* The code corresponds to Figure C6.
*Source:* WRI.

## Sectoral withdrawal

Water withdrawal in PCR-GLOBWB 2 equals gross demand unless water is unavailable. If the latter is the case, the withdrawal is lowered to match available water, and sectoral withdrawals are proportionate to the sectoral gross demand. The available water is determined by pooling ground and surface water over abstraction zones. An abstraction zone is a 1 × 1 arc degree grid cell truncated by basin and country.[20]

There are three "sources" to satisfy water demand within an abstraction zone: surface water, groundwater, and desalinated water. We assume that all the desalinated water is used first. The remaining demand is satisfied according to relative availability of surface and groundwater (renewable and fossil). There are exceptions for urban and irrigation areas where different allocation schemes are used (see Sutanudjaja et al. 2018).

Groundwater abstraction is further limited by pumping capacity, which is taken as groundwater withdrawal for the year 2000 as reported in IGRAC (n.d.). The year 2000 is taken as reference year and pumping capacities for other years estimated based on relative changes in total water demand, taking into account the trends of domestic and industrial water demand and irrigated area.

## Surface water routing module

In the Aqueduct run of PCR-GLOBWB 2, surface water is routed using a kinematic wave approximation of the Saint-Venant equations with flow described using Manning's equation. For more details and assumptions, see Sutanudjaja et al. (2018).

Lakes and reservoirs are included in the Aqueduct run of PCR-GLOBWB 2, and their actual storage is dynamically updated in the model. The Global Reservoir and Dam (GRanD) and GLWD databases are used to obtain locations and characteristics of reservoirs and lakes (Lehner and Döll 2004b; Lehner et al. 2011). For the Aqueduct run, lakes are modeled as broad crested weirs, and their outflow is modeled using a standard storage-outflow relationship.

Reservoirs aim to pass an average discharge while maintaining a water level between minimum and maximum storage (Wada et al. 2014b). The area of lakes and reservoirs varies according to global volume-area relationships. All water bodies are susceptible to open water evaporation.

The Aqueduct run of PCR-GLOBWB 2 uses a daily time step. The states of the different modules of the model—including net and gross sectoral withdrawal, river discharge, and so on—are reported on a monthly scale.

For model validation, calibration, limitations, and discussion, see Sutanudjaja et al. (2018). The model setup files, input, intermediate, and result data can be found in our GitHub repo.

## APPENDIX D: DELTA SUB-BASINS

The underlying digital elevation models of PCR-GLOBWB 2 and HydroBASINS assume a strictly convergent flow, which in some cases leads to erroneous results. Rivers will sometimes bifurcate, especially in flat delta areas. Available water resources and water withdrawal are pooled within each sub-basin. Therefore, sub-basins that are part of the same delta need to be grouped and assumed to belong to a common hydrological unit.

The previous version of Aqueduct uses sub-basins derived from the Global Drainage Basin Database (GDBD) (Masutomi et al. 2009). By default, GDBD does not contain information about which basins were grouped. According to the author of GDBD, it is not possible to replicate the delta grouping using the HydroBASINS data set. Therefore, additional information regarding the 67 delta basins[21] in GDBD was obtained directly from the authors and joined to the original database.

The process of finding and grouping delta HydroBASINS includes a semiautomated way to create a shortlist for potential delta sub-basins, and a manual step to ensure the correct classification.

To classify HydroBASINS into delta regions, a spatial join was performed between HydroBASIN level 6 and GDBD with delta classifier information. The HydroBASINS that intersect the GDBD delta basins are put on a shortlist for further inspection.

The second step is to count the number of separate GDBD streams in each sub-basin. Multiple streams are an indication for delta sub-basins.

As a third step, each shortlisted delta sub-basin is manually checked by comparing the shortlisted sub-basins with all water bodies extracted from OpenStreetMaps and the flow direction and flow accumulation of both HydroBASINS and PCR-GLOBWB 2 (OpenStreetMap contributors 2018; Lehner and Grill 2013; Sutanudjaja et al. 2018).

In total, 196 HydroBASINS are grouped into 63 delta basins. Eighty-nine delta regions have been examined. A column containing delta information is added to the final Aqueduct database.

## ENDNOTES

1. We used time series of groundwater heads. Groundwater head is a measure of pressure and can be linked to groundwater tables. See the groundwater table decline indicator for more information.
2. See Appendix A for the terminology.
3. See Appendix A for the terminology.
4. This includes direct runoff, storm flow, base flow, and return flow. For more detail, see Appendix C.
5. Water that is being transported from one basin to another other than natural flow.
6. Using the World Eckert IV projection.
7. This corresponds to one 5 arc minute cell.
8. Sinks are the most downstream cells in a routing network. This can be an ocean or an inland lake (endorheic). We used the sinks as determined by PCR-GLOBWB 2.
9. Both near-real-time and historical assessments are possible future projects.
10. The irrigation withdrawal is especially sensitive to climate forcing and evapotranspiration algorithm limitations.
11. For instance, the value for available water in 2013 is calculated by fitting an OLS regression to the 2004–13 (10-year) available water data. Finally, we take the value of the regression function for the target year: $y = f(2013)$.
12. Baseline water stress and baseline water depletion use a fraction approach. When the denominator is very close to zero, the value will be extremely high and is often based on only a few data points. Please see the indicator sections and the respective equations.
13. Environmental flow requirements are implicitly considered in the thresholds.
14. At 5x5 arc minute.
15. Our research partners at Deltares and Utrecht University ran the model for 1960–2014 but only 1990–2014 has been used to calculate the indicator. The reason is that groundwater development began to increase late 1980s and 1990s in some countries that use groundwater intensively. We assume this period to be representative of the current trend; however, further optimization might provide better insights as to the best range. Although this is different from some other indicators, we are consistently calculating baseline scores, thereby making it possible to aggregate various temporal ranges.
16. The vulnerability of people to floods is assessed as a binary condition: they are either flooded or they are not.
17. The vulnerability of people to floods is assessed as a binary condition: they are either flooded or they are not.
18. These elements are indirectly covered in the Regulatory and Reputational Risk group.
19. Or interflow.
20. Note that the default parametrization of PCRGLOWB 2 uses 30 arc minute instead of 1 arc degree abstraction zones for groundwater. In the Aqueduct run, both surface water and groundwater abstraction zones are $1 \times 1$ arc degree and truncated by basin and country.
21. Boolean classification. Sub-basin is delta or no delta.

# REFERENCES


Allen, R.G., L.S. Pereira, D. Raes, M. Smith, and others. 1998. "Crop Evapotranspiration: Guidelines for Computing Crop Water Requirements." FAO Irrigation and Drainage Paper 56.

"AQUASTAT." n.d. http://www.fao.org/nr/water/aquastat/main/index.stm. Accessed February 13, 2019.

Batjes, N.H. 2012. "ISRIC-WISE Derived Soil Properties on a 5 by 5 Arc-Minutes Global Grid (Ver. 1.2)." ISRIC-World Soil Information.

BGR and UNESCO (Bundesanstalt für Geowissenschaften und Rohstoffe and United Nations Educational, Scientific, and Cultural Organization). 2018. "Groundwater Resources of the World." https://www.whymap.org/whymap/EN/Maps_Data/Gwrw/gwrw_node_en.html.

Billen, G., and J. Garnier. 2007. "River Basin Nutrient Delivery to the Coastal Sea: Assessing Its Potential to Sustain New Production of Non-siliceous Algae." *Marine Chemistry* 106 (1–2): 148–60. doi:10.1016/j.marchem.2006.12.017.

Bouwman, A., T. Kram, and K. Klein Goldewijk. 2006. "Integrated Modelling of Global Environmental Change." *Overview of IMAGE* 2 (4): 225–28.

Bouwman, A.F., A.H.W. Beusen, J.A. Harrison, and D.C. Reed. 2015. "Nutrient Release in Global Coastal Marine Ecosystems, and Modeling of Impacts (Hypoxia, Harmful Algal Blooms and Fisheries) in Relation to Coastal Conditions." Global Foundations for Reducing Nutrient Enrichment and Oxygen Depletion from Land Based Pollution, in Support of Global Nutrient Cycle. Global Environment Facility, United Nations Development Programme, and Intergovernmental Oceanographic Commission. https://www.thegef.org/project/global-foundations-reducing-nutrient-enrichment-and-odflb-pollution-support-gnc.

Brauman, K.A., B.D. Richter, S. Postel, M. Malsy, and M. Flörke. 2016. "Water Depletion: An Improved Metric for Incorporating Seasonal and Dry-Year Water Scarcity into Water Risk Assessments." *Elementa: Science of the Anthropocene* 4 (January): 000083. doi:10.12952/journal.elementa.000083.

Carrão, H., G. Naumann, and P. Barbosa. 2016. "Mapping Global Patterns of Drought Risk: An Empirical Framework Based on Sub-national Estimates of Hazard, Exposure and Vulnerability." *Global Environmental Change* 39 (July): 108–24. doi: 10.1016/j.gloenvcha.2016.04.012.

Dalkey, N., and O. Helmer. 1963. "An Experimental Application of the DELPHI Method to the Use of Experts." *Management Science* 9 (3): 458–67. doi:10.1287/mnsc.9.3.458.

Dee, D.P., S.M. Uppala, A.J. Simmons, P. Berrisford, P. Poli, S. Kobayashi, U. Andrae, et al. 2011. "The ERA-Interim Reanalysis: Configuration and Performance of the Data Assimilation System." *Quarterly Journal of the Royal Meteorological Society* 137 (656): 553–97. doi:10.1002/qj.828.

de Graaf, I., E. Sutanudjaja, L. Van Beek, and M. Bierkens. 2015. "A High-Resolution Global-Scale Groundwater Model." *Hydrology and Earth System Sciences* 19 (2): 823–37.

de Graaf, I.E.M., R.L.P.H. van Beek, T. Gleeson, N. Moosdorf, O. Schmitz, E.H. Sutanudjaja, and M.F.P. Bierkens. 2017. "A Global-Scale Two-Layer Transient Groundwater Model: Development and Application to Groundwater Depletion." *Advances in Water Resources* 102 (April): 53–67. doi:10.1016/j.advwatres.2017.01.011.

Doorenbos, J., and W. Pruitt. 1977. "Crop Water Requirements." Irrigation and Drainage Paper No. 24. Rome: FAO (Food and Agriculture Organization of the United Nations).

EOG and NOAA (Earth Observation Group and National Oceanic and Atmospheric Administration). n.d. "Nighttime Lights." NOAA. https://ngdc.noaa.gov/eog/viirs/download_dnb_composites.html. Accessed February 13, 2019.

Eisner, S. 2016. "Comprehensive Evaluation of the WaterGAP3 Model across Climatic, Physiographic, and Anthropogenic Gradients." PhD diss., University of Kassel.

"FAOSTAT." 2012. FAO (Food and Agriculture Organization of the United Nations). http://faostat.fao.org/. Accessed February 12, 2019.

"GADM Metadata." n.d. https://gadm.org/metadata.html. Accessed February 11, 2019.

Galvis Rodríguez, S., E.H. Sutanudjaja, and M. Faneca Sànchez. 2017. "Memo: Update on the Groundwater Risk Indicators." Memo. Delft, the Netherlands: Deltares.

Garnier, J., A. Beusen, V. Thieu, G. Billen, and L. Bouwman. 2010. "N:P:Si Nutrient Export Ratios and Ecological Consequences in Coastal Seas Evaluated by the ICEP Approach." *Global Biogeochemical Cycles* 24 (4). doi:10.1029/2009GB003583.

Gassert, F., M. Luck, M. Landis, P. Reig, and T. Shiao. 2014. "Aqueduct Global Maps 2.1: Constructing Decision-Relevant Global Water Risk Indicators." World Resources Institute. https://wriorg.s3.amazonaws.com/s3fs-public/Aqueduct_Global_Maps_2.1-Constructing_Decicion-Relevant_Global_Water_Risk_Indicators_final_0.pdf.

Gesch, D.B., K.L. Verdin, and S.K. Greenlee. 1999. "New Land Surface Digital Elevation Model Covers the Earth." *Eos, Transactions, American Geophysical Union* 80 (6): 69. doi:10.1029/99EO00050.

"GLCC 2.0." 2010. U.S. Geological Survey. http://edcwww.cr.usgs.gov/landdaac/glcc/globdoc1_2.html.

Hagemann, S. 2002. "An Improved Land Surface Parameter Dataset for Global and Regional Climate Models." Max-Planck-Institut für Meteorologie, January. doi:10.17617/2.2344576.

Hagemann, S., and L.D. Gates. 2003. "Improving a Subgrid Runoff Parameterization Scheme for Climate Models by the Use of High Resolution Data Derived from Satellite Observations." *Climate Dynamics* 21 (3–4): 349–59. doi:10.1007/s00382-003-0349-x.

Harris, I., P.D. Jones, T.J. Osborn, and D.H. Lister. 2014. "Updated High-Resolution Grids of Monthly Climatic Observations: The CRU TS3.10 Dataset: UPDATED HIGH-RESOLUTION GRIDS OF MONTHLY CLIMATIC OBSERVATIONS." *International Journal of Climatology* 34 (3): 623–42. doi:10.1002/joc.3711.

Hartmann, J., and N. Moosdorf. 2012. "The New Global Lithological Map Database GLiM: A Representation of Rock Properties at the Earth Surface." *Geochemistry, Geophysics, Geosystems* 13 (12). https://agupubs.onlinelibrary.wiley.com/doi/10.1029/2012GC004370.

IGRAC (International Groundwater Resources Assessment Centre). n.d. "Global Groundwater Information System (GGIS)." https://www.un-igrac.org/global-groundwater-information-system-ggis. Accessed February 13, 2019.

IOC-UNESCO and UNEP (Intergovernmental Oceanographic Commission and United Nations Environment Programme). 2016. "Large Marine Ecosystems: Status and Trends." Nairobi: UNEP. http://geftwap.org/water-systems/large-marine-ecosystems.

Kraijenhoff van de Leur, D.A. 1958. "A Study of Non-steady Groundwater Flow with Special Reference to a Reservoir Coefficient." *De Ingenieur*, 19: B87–B94.

Lehner, B., and P. Döll. 2004a. "Development and Validation of a Global Database of Lakes, Reservoirs and Wetlands." *Journal of Hydrology* 296 (1–4): 1–22.

Lehner, B., and P. Döll. 2004b. "Development and Validation of a Global Database of Lakes, Reservoirs and Wetlands." *Journal of Hydrology* 296 (1–4): 1–22. doi:10.1016/j.jhydrol.2004.03.028.

Lehner, B., and G. Grill. 2013. "Global River Hydrography and Network Routing: Baseline Data and New Approaches to Study the World's Large River Systems." *Hydrological Processes* 27 (15): 2171–86.

Lehner, B., K. Verdin, and A. Jarvis. 2008. "New Global Hydrography Derived from Spaceborne Elevation Data." *Eos, Transactions, American Geophysical Union* 89 (10): 93. doi:10.1029/2008EO100001.

Lehner, B., C.R. Liermann, C. Revenga, C. Vörösmarty, B. Fekete, P. Crouzet, P. Döll, et al. 2011. "High-Resolution Mapping of the World's Reservoirs and Dams for Sustainable River-Flow Management." *Frontiers in Ecology and the Environment* 9 (9): 494–502.

Masutomi, Y., Y. Inui, K. Takahashi, and Y. Matsuoka. 2009. "Development of Highly Accurate Global Polygonal Drainage Basin Data." *Hydrological Processes* 23 (4): 572–84. doi:10.1002/hyp.7186.

Mayorga, E., S.P. Seitzinger, J.A. Harrison, E. Dumont, A.H.W. Beusen, A.F. Bouwman, B.M. Fekete, et al. 2010. "Global Nutrient Export from WaterSheds 2 (NEWS 2): Model Development and Implementation." *Environmental Modelling & Software* 25 (7): 837–53. doi:10.1016/j.envsoft.2010.01.007.

Meyer, V., D. Haase, and S. Scheuer. 2009. "Flood Risk Assessment in European River Basins—Concept, Methods, and Challenges Exemplified at the Mulde River." *Integrated Environmental Assessment and Management* 5 (1): 17–26. doi:10.1897/IEAM_2008-031.1.

Müller Schmied, H., S. Eisner, D. Franz, M. Wattenbach, F.T. Portmann, M. Flörke, and P. Döll. 2014. "Sensitivity of Simulated Global-Scale Freshwater Fluxes and Storages to Input Data, Hydrological Model Structure, Human Water Use and Calibration." *Hydrology and Earth System Sciences* 18 (9): 3511–38. doi:10.5194/hess-18-3511-2014.

Nachtergaele, F., H. van Velthuizen, L. Verelst, N. Batjes, K. Dijkshoorn, V. van Engelen, G. Fischer, et al. 2009. "Harmonized World Soil Database." Wageningen, the Netherlands: ISRIC.

OpenStreetMap contributors. 2018. Planet Dump. https://Planet.Osm.Org.

Portmann, F.T., S. Siebert, and P. Döll. 2010. "MIRCA2000-Global Monthly Irrigated and Rainfed Crop Areas around the Year 2000: A New High-Resolution Data Set for Agricultural and Hydrological Modeling: MONTHLY IRRIGATED AND RAINFED CROP AREAS." *Global Biogeochemical Cycles* 24 (1): n/a-n/a. doi:10.1029/2008GB003435.

Reig, P., T. Shao, and F. Gassert. 2013. "Aqueduct Water Risk Framework." Working paper. Washington, DC: World Resources Institute. https://wriorg.s3.amazonaws.com/s3fs-public/aqueduct_water_risk_framework.pdf.

RepRisk. n.d. "RepRisk ESG Data Science and Quantitative Solutions." www.reprisk.com.

Rodell, M., P.R. Houser, U. Jambor, J. Gottschalck, K. Mitchell, C.-J. Meng, K. Arsenault, et al. 2004. "The Global Land Data Assimilation System." *Bulletin of the American Meteorological Society* 85 (3): 381–94. doi:10.1175/BAMS-85-3-381.

Rohwer, J., D. Gerten, and W. Lucht. 2007. *Development of Functional Irrigation Types for Improved Global Crop Modelling*. PIK Report.

Rowe, G., and G. Wright. 1999. "The Delphi Technique as a Forecasting Tool: Issues and Analysis." *International Journal of Forecasting* 15 (4): 353–75. doi:10.1016/S0169-2070(99)00018-7.

Scussolini, P., J.C.J.H. Aerts, B. Jongman, L.M. Bouwer, H.C. Winsemius, H. de Moel, and P.J. Ward. 2016. "FLOPROS: An Evolving Global Database of Flood Protection Standards." *Natural Hazards and Earth System Sciences* 16 (5): 1049–61. doi:10.5194/nhess-16-1049-2016.

Shiklomanov, I. 1997. "Comprehensive Assessment of the Freshwater Resources of the World." Stockholm: World Meteorological Organization.

Siebert, S., and P. Döll. 2010. "Quantifying Blue and Green Virtual Water Contents in Global Crop Production as Well as Potential Production Losses without Irrigation." *Journal of Hydrology* 384 (3–4): 198–217. doi:10.1016/j.jhydrol.2009.07.031.

Steinfeld, H., P. Gerber, T.D. Wassenaar, V. Castel, M. Rosales M., and C. de Haan. 2006. *Livestock's Long Shadow: Environmental Issues and Options*. Rome: FAO (Food and Agriculture Organization of the United Nations).

Strahler, A.N. 1957. "Quantitative Analysis of Watershed Geomorphology." *Eos, Transactions, American Geophysical Union* 38 (6): 913–20.

Sutanudjaja, E.H., R. van Beek, N. Wanders, Y. Wada, J.H.C. Bosmans, N. Drost, R.J. van der Ent, et al. 2018. "PCR-GLOBWB 2: A 5 Arcmin Global Hydrological and Water Resources Model." *Geoscientific Model Development* 11 (6): 2429–53. doi:10.5194/gmd-11-2429-2018.

Todini, E. 1996. "The ARNO Rainfall: Runoff Model." *Journal of Hydrology* 175 (1): 339–82. doi:10.1016/S0022-1694(96)80016-3.

Triantaphyllou, E. 2010. *Multi-criteria Decision Making Methods: A Comparative Study*. Applied Optimization 44. Dordrecht, the Netherlands: Kluwer.

UNEP (United Nations Environment Programme). n.d. "UNEP." https://www.unenvironment.org/. Accessed on February 28, 2019.

Vanham, D., A.Y. Hoekstra, Y. Wada, F. Bouraoui, A. de Roo, M.M. Mekonnen, W.J. van de Bund, et al. 2018. "Physical Water Scarcity Metrics for Monitoring Progress towards SDG Target 6.4: An Evaluation of Indicator 6.4.2 'Level of Water Stress.'" *Science of the Total Environment* 613–14 (February): 218–32. doi:10.1016/j.scitotenv.2017.09.056.

van Huijstee, J. B. van Bemmel, A. Bouwman, and F. van Rijn. 2018. "Towards an Urban Preview: Modelling Future Urban Growth with 2UP." 3255. The Hague: PBL Netherlands Environmental Assessment Agency. https://www.pbl.nl/en/publications/towards-an-urban-preview.

van Vuuren, D.P. P.L. Lucas, and H. Hilderink. 2007. "Downscaling Drivers of Global Environmental Change: Enabling Use of Global SRES Scenarios at the National and Grid Levels." *Global Environmental Change: Uncertainty and Climate Change Adaptation and Mitigation* 17 (1): 114–30. doi:10.1016/j.gloenvcha.2006.04.004.

Verdin, K.L., and S. Greenlee. 1996. "Development of Continental Scale Digital Elevation Models and Extraction of Hydrographic Features." In *Proceedings, Third International Conference/Workshop on Integrating GIS and Environmental Modeling, Santa Fe, New Mexico*, 21–26.

Vörösmarty, C.J., B.M. Fekete, M. Meybeck, and R.B. Lammers. 2000. "Global System of Rivers: Its Role in Organizing Continental Land Mass and Defining Land-to-Ocean Linkages." *Global Biogeochemical Cycles* 14 (2): 599–621. doi:10.1029/1999GB900092.

Vörösmarty, C.J., C. Léveque, C. Revenga, R. Bos, C. Caudill, J. Chilton, E. Douglas, et al. 2005. "Millennium Ecosystem Assessment Volume 1: Conditions and Trends," chap. 7, "Freshwater Ecosystems." *Millennium Ecosystem Assessment* 1: 165–207.

Wada, Y., L.P.H. van Beek, and M.F.P. Bierkens. 2011a. "Modelling Global Water Stress of the Recent Past: On the Relative Importance of Trends in Water Demand and Climate Variability." *Hydrology and Earth System Sciences* 15 (12): 3785–808. doi:10.5194/hess-15-3785-2011.

Wada, Y., L.P.H. van Beek, D. Viviroli, H.H. Dürr, R. Weingartner, and M.F.P. Bierkens. 2011b. "Global Monthly Water Stress: 2. Water Demand and Severity of Water Stress: GLOBAL MONTHLY WATER STRESS, 2." *Water Resources Research* 47 (7). doi:10.1029/2010WR009792.

Wada, Y., D. Wisser, and M.F.P. Bierkens. 2014a. "Global Modeling of Withdrawal, Allocation and Consumptive Use of Surface Water and Groundwater Resources." *Earth System Dynamics* 5 (1): 15–40. doi:10.5194/esd-5-15-2014.

Wada, Y., D. Wisser, and M.F.P. Bierkens. 2014b. "Global Modeling of Withdrawal, Allocation and Consumptive Use of Surface Water and Groundwater Resources." *Earth System Dynamics* 5 (1): 15–40. doi:10.5194/esd-5-15-2014.

Ward, P.J., H.C. Winsemius, S. Kuzma, T. Luo, M.F.P. Bierkens, A. Bouwman, H. de Moel, et al. Forthcoming. "Aqueduct Floods Methodology." Technical Note. Washington, DC: World Resources Institute.

Weedon, G.P., G. Balsamo, N. Bellouin, S. Gomes, M.J. Best, and P. Viterbo. 2014. "The WFDEI Meteorological Forcing Data Set: WATCH Forcing Data Methodology Applied to ERA-Interim Reanalysis Data." *Water Resources Research* 50 (9): 7505–14.

Wendling, Z.A., J.W. Emerson, D.C. Esty, M.A. Levy, and A. de Sherbinin. 2018. "2018 Environmental Performance Index." New Haven, CT: Yale Center for Environmental Law and Policy. https://epi.envirocenter.yale.edu/2018-epi-report/introduction.

Wint, W., and T.P. Robinson. 2007. *Gridded Livestock of the World, 2007*. Rome: FAO (Food and Agriculture Organization of the United Nations).

World Bank. n.d. "World Bank National Accounts Data." World Bank. https://data.worldbank.org. Accessed February 13, 2019.

WHO and UNICEF (World Health Organization and United Nations Children's Fund). 2017. *Progress on Drinking Water, Sanitation and Hygiene: 2017 Update and SDG Baselines.* https://washdata.org/.

"WRI's Open Data Commitment: World Resources Institute." n.d. https://www.wri.org/about/open-data-commitment. Accessed February 27, 2019.

WRI, UNEP, UNDP (World Resources Institute, United Nations Environment Programme, United Nations Development Programme), and World Bank, eds. 1998. *World Resources, 1998–99: A Guide to the Global Environment Environmental Change and Human Health*. New York: Oxford University Press.

Xie, H., C. Ringler, and G. Pitois. 2016. "Assessing Global BOD, Nitrogen and Phosphorus Loadings under Socioeconomic and Climate Change Scenarios." Technical note. IFPRI (International Food Policy Research Institute).

## ABOUT THE AUTHORS

**Rutger W. Hofste** is an associate with WRI's Water Program, where he develops the new Aqueduct water risk information platform, including a suite of online tools and a water risk database. His responsibilities include working with various research organizations and tool developers as well as doing large-scale, cloud-based, hydrological data processing.

**Samantha Kuzma** is a GIS research analyst with WRI's Water Program. Her primary tasks include data analytics, geospatial analysis, and data visualization.

**Sara Walker** is a senior manager for water quality and agriculture in WRI's Water Program. She leads the Institute's global water quality work, including mapping and measuring eutrophication and advancing innovative policy approaches like water quality trading to cost-effectively reduce nutrient pollution.

**Edwin H. Sutanudjaja** is the core developer of PCR-GLOBWB 2 in the Department of Physical Geography at Utrecht University.

**Marc F. P. Bierkens** is a professor of hydrology at Utrecht University, where he holds the Chair of Earth Surface Hydrology in the Department of Physical Geography. He is also a senior scientist at Deltares.

**Marijn J. M. Kuijper** is the head of the Department of Groundwater Management at Deltares.

**Marta Faneca Sanchez** is a hydrogeologist at Deltares.

**Rens van Beek** is an assistant professor of large-scale hydrology and Earth surface processes at Utrecht University.

**Yoshihide Wada** is acting director of IIASA's Water Program. He has a joint appointment as a Chair Professor of Water and Food Security at Utrecht University, an adjunct research scientist at the Center for Climate Systems Research at Columbia University, and an adjunct professor at the School of Geographic Sciences, East China Normal University.

**Sandra Galvis Rodríguez** is an advisor in the subsurface and groundwater systems unit at Deltares.

**Paul Reig** is a director in WRI's Water Program and responsible for managing WRI's corporate engagement on water and the Aqueduct Water Risk Atlas. As a thought leader in corporate water stewardship and data analytics, his work helps drive sustainable business growth in a water-constrained world.

## ACKNOWLEDGMENTS

We are pleased to acknowledge our institutional strategic partners, who provide core funding to WRI: Netherlands Ministry of Foreign Affairs, Royal Danish Ministry of Foreign Affairs, and Swedish International Development Cooperation Agency.

This publication was made possible thanks to the support of the Aqueduct Alliance (Dutch Ministry of Infrastructure and Water Management, Bloomberg LP, Cargill Inc., DuPont, Ecolab Inc., General Motors Company, Kimberly Clark Corporation, Proctor & Gamble Company, Skoll Global Threats Fund, Tyson Foods Inc.). Additionally, we thank the World Bank for supporting parts of Aqueduct Floods.

The authors would like to thank the following people for providing invaluable insight and assistance in their reviews of this report: Arthur Beusen (Utrecht University), Alexander Bouwman (Utrecht University), Laura Malaguzzi (WRI), Gustavo Naumann (JRC), Betsy Otto (WRI), Leah Schleifer (WRI), Emilia Suarez (WRI), Timothy Tiggeloven (IVM), Philip Ward (IVM), Hessel Winsemius (Delft University of Technology), and Hua Xie (IFPRI); as well as our internal reviewers Zablon Adane, Deepak Sriram Krishnan, Tianyi Luo, Carolyn Savoldelli, Jiao Wang, and Lihuan Zhou; and external reviewers John Hollerung (Nike), Sarah Elaine Lewis (The Sustainability Consortium), Tom Parris (iSciences), and Adam Schlosser (MIT).

The authors would also like to thank our research partners at Deltares, IFPRI, IVM, RepRisk, and Utrecht University, as well as Vizzuality, Romain Warnault, Carni Klirs, and Billie Kanfer for their extensive guidance and feedback during the design and development of this study.

Opinions or points of view expressed in this report are those of the authors and do not necessarily reflect the position of the reviewers, research partners, or the organizations they represent.


## ABOUT WRI

World Resources Institute is a global research organization that turns big ideas into action at the nexus of environment, economic opportunity, and human well-being.

**Our Challenge**

Natural resources are at the foundation of economic opportunity and human well-being. But today, we are depleting Earth's resources at rates that are not sustainable, endangering economies and people's lives. People depend on clean water, fertile land, healthy forests, and a stable climate. Livable cities and clean energy are essential for a sustainable planet. We must address these urgent, global challenges this decade.

**Our Vision**

We envision an equitable and prosperous planet driven by the wise management of natural resources. We aspire to create a world where the actions of government, business, and communities combine to eliminate poverty and sustain the natural environment for all people.

**Our Approach**

COUNT IT

We start with data. We conduct independent research and draw on the latest technology to develop new insights and recommendations. Our rigorous analysis identifies risks, unveils opportunities, and informs smart strategies. We focus our efforts on influential and emerging economies where the future of sustainability will be determined.

CHANGE IT

We use our research to influence government policies, business strategies, and civil society action. We test projects with communities, companies, and government agencies to build a strong evidence base. Then, we work with partners to deliver change on the ground that alleviates poverty and strengthens society. We hold ourselves accountable to ensure our outcomes will be bold and enduring.

SCALE IT

We don't think small. Once tested, we work with partners to adopt and expand our efforts regionally and globally. We engage with decision-makers to carry out our ideas and elevate our impact. We measure success through government and business actions that improve people's lives and sustain a healthy environment.

Maps are for illustrative purposes and do not imply the expression of any opinion on the part of WRI, concerning the legal status of any country or territory or concerning the delimitation of frontiers or boundaries.